UNIVERSITY OF LIVERPOOL – SURFACE SCIENCE RESEARCH CENTRE

Study of the surface structure of i-Ag-In-Yb quasicrystal and the thin film growth of Cu

Chris Hodson

A dissertation submitted for MPhys Degree at Department of Physics of the University of Liverpool

Contents

Abstract

In this study, the five-fold surface of icosahedral Ag-In-Yb has been studied using different techniques, namely low energy electron diffraction (LEED) and scanning tunnelling microscopy (STM). It is found that the clean surface displays terraces and step formation and has been analysed and compared with results from a previous sample. Depending on the bias voltage applied the STM images are characterised by either pentagonally arranged protrusions or rings observed at the vertices of these pentagons. Like other previously studied samples the clean surface exhibits quasiperiodical order. The size and separation of the protrusions and the diameters of the rings have been measured from STM analysis. An over-layer of Cu was also deposited on the *i*-Ag-In-Yb surface leading to measurements of the size and height of the Cu clusters at high and low coverage. The analysis of the Cu deposition suggests that Cu prefers to form in 3-D islands above certain coverage.

1 Introduction

Icosahedral quasicrystals differ from conventional crystals as they possess long rang order without any periodicity and exhibit rotational symmetries with quasiperiodical order [1]. It is whether the quasiperiodicity influences the physical properties and characteristics of the material that is attracting interest in this field. Understanding the atomic structure of the surface is essential to achieve an insight into unusual surface properties of quasicrystals such as low friction and very low zero-temperature conductivity. Surface properties are related to potential technological applications such as coating, catalysts and thin film growth. The quasicrystal surfaces can also be used as a template to grow an atomic or molecular over-layer, for example, a pseudomorphic film of a single element [2].

The ultimate aim is to produce a single element over layer and due to the reduced chemical complexity investigate the effect of quasiperiodicity on the characteristics of a material. The study of *i*-Ag-In-Yb took place in Ultra High Vacuum conditions as the quasicrystal would be oxidised in air forming an oxide layer. An atomically flat surface for the *i*-Ag-In-Yb can be achieved using the sputter-annealing process. Due to the different chemical composition of *i*-Ag-In-Yb compared to that of previous Al-based samples, this new class of Ag-based quasicrystals will show different chemical and structural properties to those previously seen and therefore different surface properties.

Up until recently quasicrystal studies were limited to Al-based crystals where the system structure is best represented in terms of pseudo-Mackay Icosahedron (PMI) and Bergman clusters [2]. The *i*-Ag-In-Yb sample is isostructural to the *i*-Cd-Yb quasicrystal where the structure is as an

aperiodic arrangement of rhombic tricontahedral (RTH) clusters [2]. Under UHV conditions the Cd evaporates under an increase in temperature which makes it unsuitable for surface preparation. The discovery of *i*-Ag-In-Yb has provided a solution to the study of this family of quasicrystals. The Cd replaced by equal percentages of UHV stable Ag and In maintained the valance electron atomic ratio of 2.0 necessary for the formation of these crystals [1]. The *i*-Ag-In-Yb sample used for this study was grown using the Bridgman method giving the composition *i*-$Ag_{42}In_{42}Yb_{16}$ and was cut in the five-fold axis determined by Laue backscattering [3].

Using both LEED and STM techniques the clean surface structure of *i*-Ag-In-Yb was found to exhibit long range aperiodic order with forbidden symmetry. The STM images showed the clean surface to form in steps and terraces. Using negative and positive bias voltages, the STM images of the terraces displayed characteristic protrusions and rings comparable to previously studied samples. After deposition of a Cu atomic over-layer on the *i*-Ag-In-Yb surface, the analysis of the thin film suggests long range quasiperiodic order similar to that of the clean surface may be present. Further LEED analysis of the Cu over-layer is needed to confirm this.

2 Background Information

2.1 Solids, Crystals and Crystallography

When solids are formed, it is the variation in the rate of cooling which can enable a solid of the same material to possess a completely different structure. As a material falls below its melting point two structural states can be achieved depending on the rate of the solids energy loss. An amorphous solid can be formed from rapidly cooling high viscosity liquid. After cooling below the melting point, the random structure of the liquid is retained without any crystallisation due to the atoms or molecules being unable to move into crystal lattice sites. There are no repeat patterns within the structure and therefore no long range translational order, short range order may exist, but is restricted to the nearest neighbouring atoms. If a material is cooled from a melt (liquid) more slowly below its melting point under carefully controlled conditions, then a highly ordered crystal structure can be grown which will possess repeated geometric patterns.

Any crystalline structure will possess coherent atomic order. The crystal will be made up of repeat periodic arrangements of one or multiple atoms repeated around a lattice point. The lattice point is defined as the origin of the unit cell for a given material. The unit cell is used to describe the spatial arrangement of the atoms within the crystal.

Using model lattices to predict the structural arrangement of crystals enables an insight in to how other crystals might form. Auguste Bravais (1811-1863) summarised in 1845 that there are only 14 lattices possible within 3 dimensional crystals. The 14 Bravais lattices, using the vectors within the unit cell are able to define the structure of the complete lattice. The crystal will look the same from any point viewed from the lattice points. To construct a classical lattice, only the basis of the crystal and the lattice point are required. The basis can be defined as the number of atoms associated with each lattice point.

All 14 of the Bravais lattices were confirmed by Max Von Laue (1879-1960) in 1912 using x-ray diffraction. Laue used light of wavelength similar to the atomic spacing to produce an interference pattern upon reflection from the material. The real space structure of the material was then determined from the reciprocal space diffraction pattern. Laue's experiment shown the 14 Bravais lattices to either have two, three, four or six-fold symmetry, therefore any rotation of 180^0, 120^0, 90^0 or 60^0 degrees would identically give the original pattern. This rotation would overlay itself identically in the reciprocal space also, prompting belief that diffraction patterns that contain no order of rotational symmetry were not possible.

2.2 The Discovery of Forbidden Symmetry

In 1982 Dan Shechtman was studying the structure of Al-Mn alloys using electron diffraction upon which he discovered a diffraction pattern with ten-fold symmetry. Due to the sharp diffractions spots the structure was not that of a glass, the sharp spots could only be produced from constructive interference within a well ordered structure. The ten-fold symmetry however did not match the translational symmetry seen in any of the conventional 14 Bravais lattices. The discovery of this "forbidden symmetry" and the observation of different rotational symmetries being seen by rotation of the crystal led Shechtman, Blech, Gratias and Cahn to deduce that the Al-Mn alloy had icosahedral point group symmetry [4].

Icosahedrons are commonly found in inner metallic crystals, where a smaller transition element is at the very centre and is surrounded by 12 larger atoms, which make up the corners of the icosahedron. Equilateral triangles make up the 20 faces of the icosahedron and it possesses five-fold, three-fold and two-fold rotational symmetry [5]. The reason the diffraction pattern observed by Shechtman appeared to be ten-fold was due to the opposite faces along the axes of symmetry being inverted, it is essentially two five-fold patterns superimposed, with the backward face 180^0 out of phase.

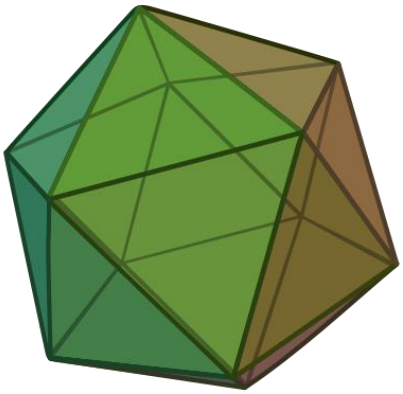

Figure 2-1 Icosahedron showing multiple rotational symmetry.

Shechtman concluded in his 1984 paper that the icosahedral phase had long-range order and no translational symmetry. The definitions of a crystal and also rotational symmetry have shifted more towards reciprocal space rather than real space. This is due to the lattice not overlaying the original pattern if rotated in real space. Since quasicrystals have been proved to have long-range order yet they do not possess periodic means that they must possess what is known as aperiodic order [4].

2.3 Aperiodic Order

2.3.1 Fibonacci Sequence

The Fibonacci sequence is one of the oldest and simplest examples of aperiodic order. The sequence is a 1 dimensional number sequence where the rule is simply "the next term in the sequence is given by the sum of previous two terms";

1, 1, 2, 3, 5, 8, 13, 21 …

In quasicrystal step terrace formation the Fibonacci sequence is expressed in terms of L and S where L is greater than S and LS is greater than L, giving;

S, L, LS, LSL, LSLLS, LSLLSLSL, LSLLSLSLLSLLS…

As the numbers become larger as the Fibonacci sequence progresses, the ratio of a term to its previous term begin to approach even closer to what is known as the golden mean;

$$\tau = \frac{(1 + \sqrt{5})}{2} \approx 1.618$$

Using the previous form of the Fibonacci sequence using L and S, the ratio of L:S also approaches τ. The golden number and the Fibonacci sequence are distinctly associated to aperiodic

order. Along with the Fibonacci sequence describing the step terrace formation on the surface of quasicrystals, the golden ratio τ is commonly found in the five-fold symmetry that quasicrystals possess [2, 8].

2.3.2 Penrose Tiling's

A tiling is defined as a periodic arrangement using a finite number of polygons to fill a surface completely without any gaps. Using just the one tile whether it is rectangles, triangles, squares or hexagons periodically, a surface can be filled. Such tiling's will always possess rotational symmetry unlike aperiodic patterns. The use of just one pentagon tile will not be able to completely cover a surface; Roger Penrose in 1974 developed a tiling with five-fold rotational symmetry and no translational order using multiple tiles. This is the Penrose P1 tiling;

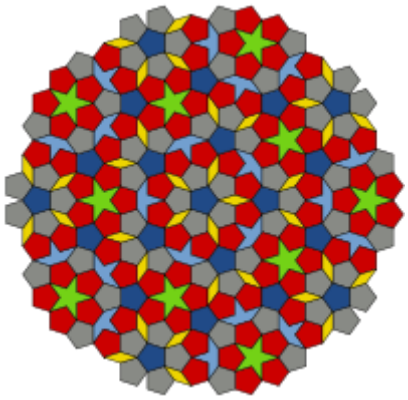

Figure 2-2 Penrose 1 tiling.

Penrose produced another tiling which consisted of two different tiles instead of four, this time using two types of rhombus. Interestingly the ratio of areas of the two rhombi is the golden ratio τ. The P3 tiling is arranged aperiodically just like the P1, and no two rhombi form a parallelogram. This allows for very few arrangements and gives no translational symmetry. Some of the repeated patterns within the P3 tile are able to produce a decagon that looks like a star and possesses perfect five-fold rotational symmetry. Any diffraction pattern taken of the P3 Penrose tiling would give five-fold symmetry and even ten-fold symmetry. Recently computational FFT analysis has shown these tiling's to have both five-fold and ten-fold symmetry.

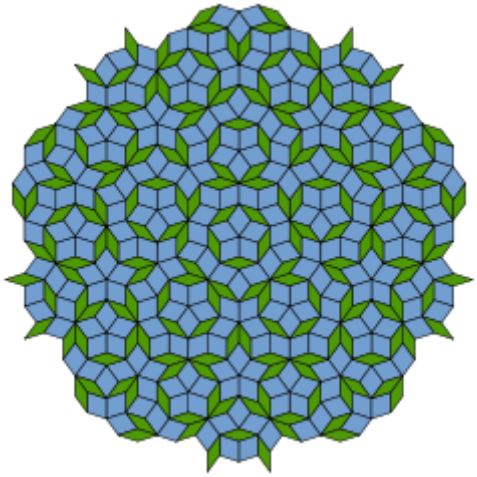

Figure 2-3 Penrose 3 tiling using “fat” and “skinny” rhombi.

Some of these Penrose tiling’s have been found to actually fit real quasicrystal images using STM. Overlaying a Penrose tile on a quasicrystal model surface has shown an exact match, where the atomic positions are placed at the vertices of the tiles [9]. These vertices where labelled by Mackay as quasi-lattice points. A real LEED pattern taken of a clean surface quasicrystal is in good comparison with the FFT’s of the Penrose tiling’s used to overlay the STM image of the sample.

3 Quasicrystals

3.1 3-D Icosahedral Quasicrystal Structure

Icosahedral quasicrystals lack periodicity in any direction and therefore they are truly aperiodic. The Al-Mn alloys that Shechtman studied were the first quasicrystals found and are part of the icosahedral quasicrystal group. There are many icosahedral Al based crystals, examples being; Al-Pd-Mn, Al-Cu-Fe and Al-Mn-Sn. Al-Pd-Mn is described as an F-type quasicrystal and has been studied the most intensively, its structure shows great comparison to that of a 3-Dimensional Penrose tiling. Clusters of atoms are arranged in such a way that they give icosahedral symmetry. The Pseudo-Mackay Icosahedron (PMI) cluster is considered to be the basic unit for the Al based quasicrystals and the Bergman clusters describe the structure of the other known alloys, specifically *i*-Ag-In-Yb for this study [1].

Mackay type; 54 atoms forming the triple shells, icosahedron, icosidodecahedron, larger icosahedron

- Al-Pd-(Mn, Re)
- Al-Cu-(Fe, Ru, Os)

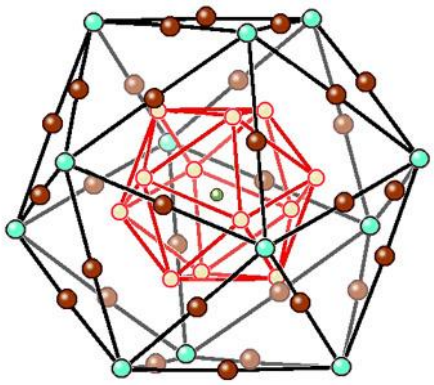

Figure 3-1 Mackay Cluster.

Bergman type; 104 atoms forming four shells, icosahedron, dodecahedron, larger icosahedron, truncated icosahedron

- Ag-In-Yb
- Cd-Yb
- Al-Li-Cu
- Zn-Mg-Ga
- Ti-Zr-Ni
- Zn-Mg-(Y, Dy, Gd, Ho, Tb, Er)

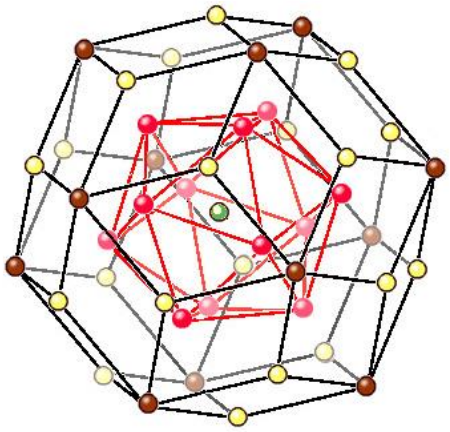

Figure 3-2 Bergman Cluster.

The clusters shown can vary in their chemical arrangement, and depending on their elemental composition, can sometimes overlap each other. The precise ratio's and arrangements of the Pseudo-Mackay Icosahedron and Bergman clusters within a quasicrystal lattice have yet to be confirmed. In some cases it is suggested that a lattice may be composed of a compound of both cluster types, with the Bergman clusters existing in the space between the PMI clusters.

3.2 Cd-Yb and Ag-In-Yb

The structural building block of the *i*-Cd-Yb quasicrystal family is the rhombic tricontrahedral (RTH) cluster. The rotational symmetry of the RTH cluster is identical to that of the icosahedron made up of equilateral triangles previously shown. The RTH cluster exhibits five-fold, three-fold and two-fold symmetry also.

Figure 3-3 Rhombic Triacontahedron.

The RTH cluster shows similar composition to that of the P3 Penrose tiling which possesses five-fold symmetry upon FFT analysis. *i*-Cd-Yb is composed of an aperiodic arrangement of these clusters. Due to the unsuitability of Cd-Yb for UHV conditions the newly discovered Ag-In-Yb has provided the possibilities for the study of new epitaxial growth phenomena [6]. Since *i*-Ag-In-Yb is icostructural to Cd-Yb it is expected to have similar structure to that presented in Figure 3-4, with the Cd replaced by equal percentages of Ag and In;

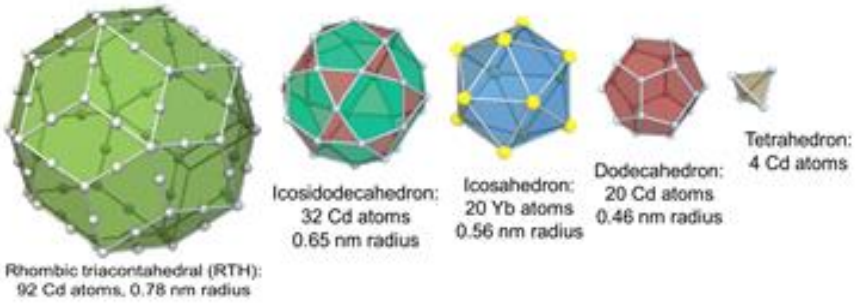

Figure 3-4 Building blocks of *i*-Cd-Yb.

4 Surface Preparation and Surface Science Techniques

4.1 Quasicrystal Surface Preparation

4.1.1 Ultra High Vacuum - UHV

All studies of quasicrystals must take place under UHV conditions so that the surface may be kept clean and protected from the contamination of unwanted gases. The ultra high vacuum also helps avoid any interference of any particles such as electrons and ions when using techniques such as LEED.

The UHV is prepared by first completing a bake out. During a bake out, the chamber is sealed and the chamber is heater up to 400-500 K for 2-3 days while the vacuum pumps are in operation. The purpose of the bake out is to enable to the desorption of water vapour and any other remaining gases from the UHV chambers internal surfaces. Once the bake out is completed, and the chamber has returned to room temperature, a pressure typically around $1 \times 10^{-10}\ mbar$ is achieved using all of the available pumps.

Figure 4-1 Photograph of VT-STM UHV set up.

The UHV chamber consists of a stainless steel chamber with metal seals to help form vacuum. The pumps used to achieve UHV conditions are Turbo pumps, Rotary pumps and Ion pumps. On the left of Figure 4-1, the window flanges can be seen, this is where the LEED optics and the STM are placed. A manipulator seen on the right is used to transfer the sample from various chambers and in to place for sputter-annealing and single element deposition.

4.1.2 Preparation of the Surface

The *i*-Ag-In-Yb sample used for this study was grown using the Bridgman method giving the composition *i*-$Ag_{42}In_{42}Yb_{16}$ and was cut in the five-fold axis determined by Laue backscattering [7]. Upon exposure to air, quasicrystals can begin to form an oxide a layer of 2-3nm thickness on the surface of the crystal. In order to study the surfaces of quasicrystals to a high degree of resolution, it is important to clean the surfaces prior to UHV conditions. To achieve high resolution images using STM, the ion bombardment process of sputtering and annealing was used to achieve an atomically flat surface.

The sample used for this study was taken from the same ingot formed from the Bridgman method used to produce the *i*-Ag-In-Yb sample used in previous studies [1]. Unlike the older crystal sample, the sample for this study underwent special treatment and was annealed for a month with the aim to produce a cleaner surface. The purpose of the special treatment for the quasicrystal is to enable atomic vacancies to migrate from the bulk to the surface by using a sufficiently high enough temperature during the annealing process.

The surface must first be polished before being place under UHV conditions using diamond paste down to 0.25μm, it is then sputtered using Ar^+ (1-3 keV for 30-60 min). The quasicrystal sample is then annealed under UHV conditions (base pressure ($2 \times 10^{-10}\ mbar$) at a suitably high enough temperature (at 650 K for *i*-AgInYb). After this first treatment, the sample is removed from UHV and polished once more in order to remove the void-rich region from the top of the surface leaving the vacancy depleted zone. The newly polished surface undergoes the full cleaning process of repeat cycles of sputtering and annealing back under UHV conditions. The sputtering process causes a depletion of In and Yb at the surface, this is due to the Ag being the lightest of the elements within the compound, the bulk composition is then restored through the annealing process [2]. A perfect quasicrystalline surface is achieved through this repeat sputter-annealing process as the quasicrystal follows the pattern of the bulk structure underneath when cooled. To record the temperature during the annealing process an optical pyrometer is used with the emissivity set to that of the i-AgInYb sample ~0.35 [7]. The sample is normally heated close to the melting point of the surface [2].

4.2 Low Energy Electron Diffraction – LEED

Low Energy Electron Diffraction uses electrons emitted from a filament, which are accelerated through a drift tube to specific required energies. The electrons will possess a de Broglie wavelength similar to that of the atomic separation so that they require the condition for Bragg diffraction. The electrons are back scattered from the crystal in preferred directions due to these Bragg diffractions conditions. The fluorescent screen collects the back scattered electrons and then accelerates the collected electrons at a biased voltage so that they reach a kinetic energy high enough to cause light emission. The x-rays produced from the filament only penetrate a few atomic layers in to the solid due to the short inelastic mean free path of the electrons. LEED is therefore surface sensitive.

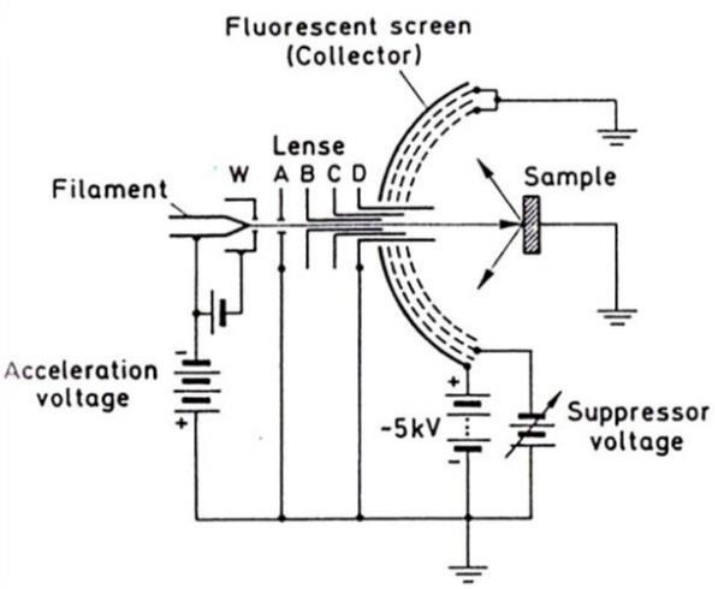

Figure 4-2 Schematic diagram of LEED setup.

There are two ways the information from LEED can be used; qualitatively and quantitatively. The first, the diffraction pattern is recorded and analysis of the spots positions produces information about the symmetry of the surface structure and the quality of the surface. In the second method; quantitative structure determination, measurements of the diffraction intensities as a function of incident electron beam energy are able generate “I-V” curves. The comparison to these models can provide accurate information about atomic positions.

4.3 Scanning Tunnelling Microscopy – STM

In 1981 the scanning tunnelling microscope was invented by Gerd Binnig and Heinrich Rohrer. Since then STM has become the most used and important tool in surface science and nanoscience research. The reason for STM's success is that it allows a real space view of the atomic configuration of conducting surfaces, whereas LEED only represents a reciprocal space view of a crystal.

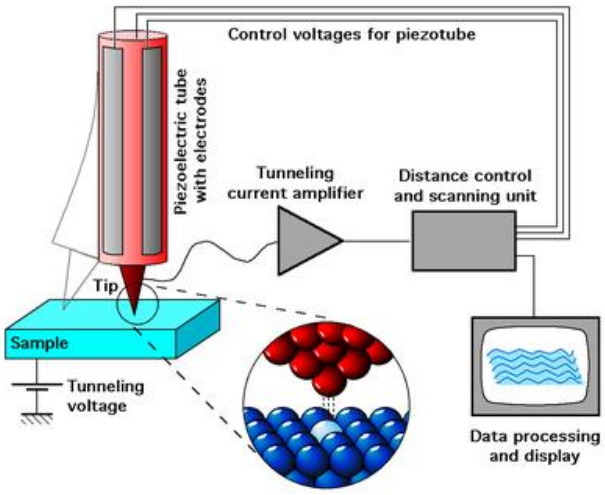

Figure 4-3 Overview of STM setup.

STM works on the principle of quantum mechanical tunnelling. Electrons are able to tunnel between the sample and an atomically sharp tip which is controlled by piezoelectric crystal. When the tip is brought very close to the surface (~1 nm) and a bias voltage is applied quantum mechanics allows the electrons to conduct across the vacuum between the tip and the sample. Using a positive sample bias, the electrons tunnel from occupied states within the tip to unoccupied states in the sample. Images using a positive bias will show the unoccupied states of the sample. Oppositely, a negative bias allows electrons to tunnel from occupied sample states to unoccupied tip states resulting in the image showing occupied sample states.

By moving the tip across the surface of the sample, the tunnelling current is measured. The tunnelling current exponentially drops upon a separation increase. The tunnelling current j is represented by the equation;

$$j = Ae^{(-\varphi d)}$$

Where A is a constant, φ is the barrier height and d is the separation between tip and sample.

The movement of the atomically sharp tip is controlled in the x-y plane using piezoelectric materials. Under an applied voltage these crystals expand by a small amount which enables a precisely controlled approach to the surface being studied. STM has two modes of operation; constant

current and constant height. Constant current mode is the most widely used and generates the highest resolution of the two modes. To keep the current constant a feedback loop is used and the tip only moves up and down in the z-direction. The tip will then scan across the surface and the date recorded will be the movement of the tip in the z-direction for each corresponding x-y position. This will enable a 3-dimensional image of the surface to compile. In contrast to constant current mode, constant height mode maintains a fixed height (z-direction) as the tip scans across the surface. The advantage of constant height mode is that the scanning speed is a lot faster than constant current mode; this however is compromised by lower resolution images. The change in the current during constant height mode, using the relation above allows for a profile of the surface to be built up.

The need for a flat clean surface for STM studies is imperative. Quasicrystals samples must undergo the intense surface preparation of polishing, sputtering and annealing so that the tip does not crash as it scans across the surface in the z-direction. If the sample surface is too rough or dirty, it is possible for the tip to "pick up" or manipulate atoms or molecules on the surface during a scan. This hinders the study of the surface topography due to the changing conductivity and tunnelling distance.

It is important to note that although STM can produce atomic resolution images of a real space surface, the images are not actually individual atoms. What is being imaged is the joint Density of States (DOS) between the tip and the sample. The current will either flow from tip to sample, or from sample to tip depending on the bias voltage. As previously stated this determines whether the electrons flow from the tip in to unoccupied sample states, or from the sample in to unoccupied tip states [1]. Changing the bias voltage due to the difference in the density of states between the tip and the sample gives two different images of the same surface position. It is the change in the density of states which create an image of the occurrence of the atoms within a given surface. For example, a region of high density of states would normally suggest the presence of atoms, although in some cases the overlapping of wave function from atomic interactions can conflict with this assumption. Despite these difficulties, STM still remains the most effective way of producing real space images of conducting surfaces.

4.4 Growth of Atomic Over-layers

The process of atoms forming a bond to a surface is known as adsorption. This is different to absorption, where the molecules may enter in to the bulk of the substrate rather than the surface. For thin-film growth, the flux of a material e.g. Cu, is produced by evaporation. This evaporation is produced by applying voltage to the material, to cause emission on to the desired surface. The atoms may then condense on the crystal surface. Some atoms, upon reaching the crystal surface may immediately re-evaporate or diffuse, however many atoms may be absorbed at specific defect sites along the surface. It is possible for some atoms to nucleate and attach to an already formed nucleus resulting in the growth of a film.

There are 3 main growth modes which may possibly occur when a material is deposited on the clean surface of another material;

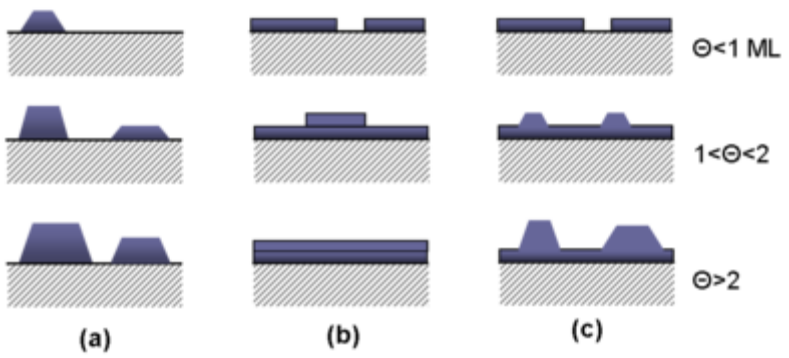

Figure 4-4 – 3 main growth modes of atomic over-layers.

4.4.1 Island Growth – Volmer-Weber (a)

A new layer begins to form before the previous layer has been completed. This results in the formation of 3-D islands on the substrate. In this case the substrate-vacuum interfacial energy is less than the sum of film-vacuum and substrate-film energy.

4.4.2 Layer by Layer Growth – Frank-van der Merve (b)

Only when a previous layer has completed its formation will a new layer start to grow. This is due to the interaction between the substrate and the film being stronger than that of the atoms in neighbouring layers. The substrate-vacuum interfacial energy is greater than the sum of film-vacuum and substrate-film energy.

4.4.3 Layer plus Island Growth – Stranksi-Krastanov (c)

The film in the layer plus island growth mode forms in 3-D islands after the complete growth of one or more monolayers previously. This is produced by a mismatch between substrate and film and cannot continue for thicker film, resulting in 3-D islands.

5 Results and Analysis

5.1 Clean Surface Study of *i*-Ag-In-Yb

As previously covered in Section 4.1.2, the *i*-Ag-In-Yb sample used for this study was cut in the five-fold axis determined by Laue backscattering. The surface was polished before being place under UHV conditions using diamond paste down to 0.25 μm, the sample was then sputtered using Ar^+ (1-3 keV for 30-60 min).

The newly polished surface underwent the full cleaning process of repeat cycles of sputtering and annealing (1keV for 30-60min under 1-2× $10^{-10} mbar$) back under UHV conditions. The *i*-Ag-In-Yb crystal after subsequent cycles was annealed at about 650 K for a month.

After the full surface preparation, the first STM images using Omicron STM at room temperature of the clean surface were taken along the *i*-AgInYb five-fold surface. The annealing process would allow the clean surface to exhibit the expected terraces and steps of different heights. Over 100 STM images of various steps and terraces from multiple locations on the surface were taken in order to determine the height distribution of the clean surface.

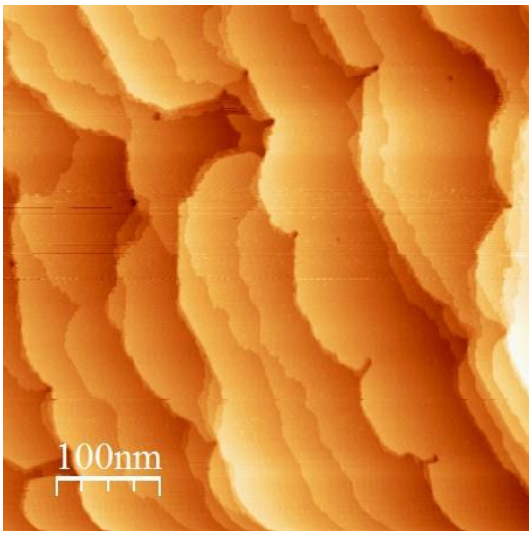

Figure 5-1 STM image of clean surface *i*-Ag-In-Yb: 500 nm x 500 nm, +1.1 V.

Figure 5-1 (500 nm x 500 nm, +1.1 V) above indicates that large terraces are formed from the preparation procedure. There is a range of step height distributions, and it is evident that there are smaller terraces in between the larger terraces. Figure 5-2 is an enlarged image of a section of Figure 5-1and shows the intermediate terraces.

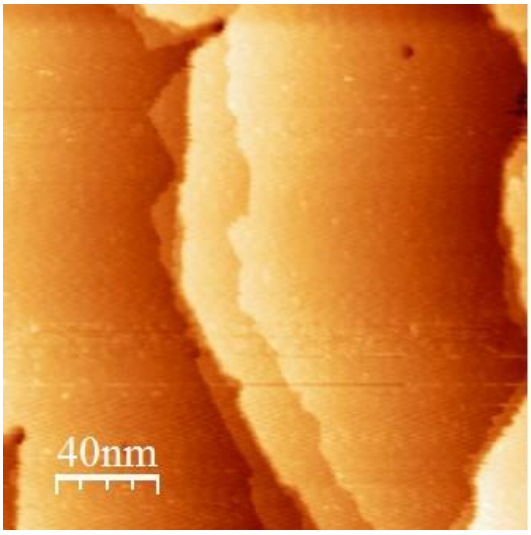

Figure 5-2 Clean surface terraces exhibiting various sized terraces of large and narrow width: 200 nm x 200 nm, +1.1 V.

The next step was to deduce the nature of symmetry of the surface. A terrace was chosen to study and images were taken even closer to the surface at a 100 nm x 100 nm scale. A Fast Fourier Transform image of Figure 5-3 would be able to provide evidence of the surface exhibiting quasicrystalline order.

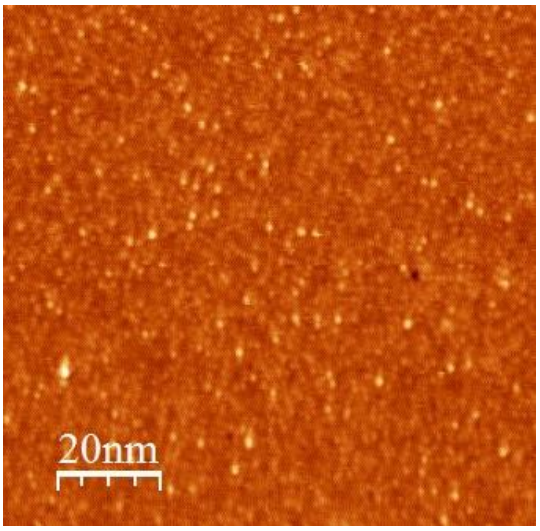

Figure 5-3 Englarged terrace image of Figure 5-2: 120 nm x 120 nm, +1.1 V.

This enlarged view of the chosen terrace shows the atomic surface structure in greater detail. The density of states of the features within the *i*-Ag-In-Yb surface become more evident.

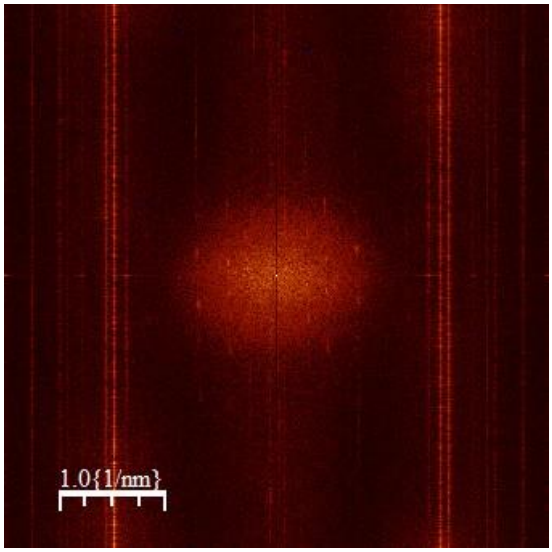

Figure 5-4 FFT of Figure 5-3 exhibiting quasiperiodic symmetry.

An FFT image (after filtering) of Figure 5-3 faintly shows two rings composing of 10 spots, indicating the forbidden symmetry expected of quasicrystalline surfaces. This confirms that the clean surface of *i*-Ag-In-Yb which represents the bulk structure fully exhibits quasiperiodic order like the Penrose 3 tiling. The terraces are formed at those planes which intersect the centre of the rhombic triacontahedral clusters perpendicular to the the five-fold axes therefore forbidden symmetry is expected in the FFT of the terrace surface [3].

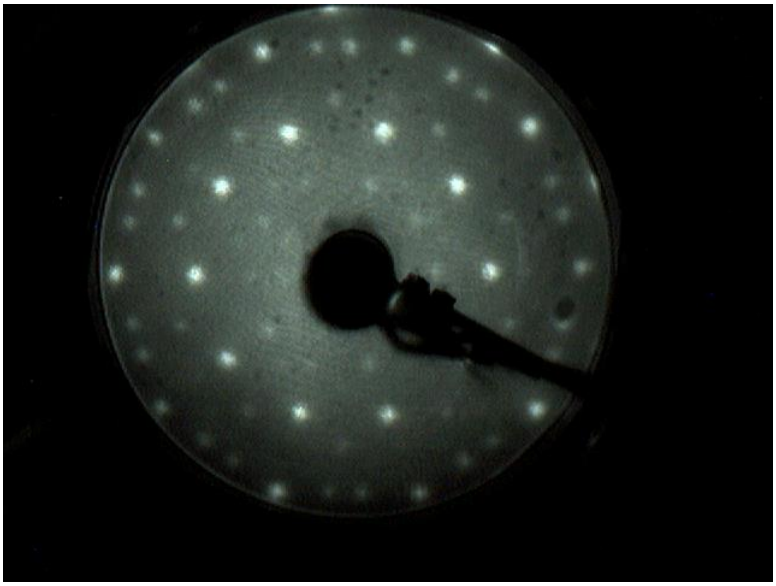

Figure 5-5 LEED image of clean surface (older sample) exhibiting distinct ten-fold symmetry: beam energy 15.1 eV.

Figure 5-5 show a LEED image of the clean surface using 15.1 eV incident beam energy, with the lens settings kept constant throughout all the LEED imaging. The pressure at the time of imaging was $5 \times 10^{-10} mbar$. As expected the LEED image shows clear quasiperiodic symmetry which again confirms the quasicrystalline nature of the *i*-Ag-In-Yb surface. It is to be noted that the LEED pattern (Figure 5-5) was obtained from the older *i*-Ag-In-Yb sample which did not undergo the special treatment of annealing for 1 month. The LEED images obtained from the sample clean surface in this study were not of the same quality as the one in Figure 5-5 and are not presented here. The special treatment of 1 month annealing was expected to produce a higher quality surface as done so in previous Al based studies. The higher quality LEED images from the old sample were produced with beam energy of 20-30 eV, with 15.1 eV used for Figure 5-5. The sample for this study required higher beam energy for LEED images at approximately 50 eV. The structure quality of the sample in this study is not of the same quality as the older sample taken from the same ingot.

It is to be noted that all FFT's were "filtered" before being computed. This was done so that when analysing the clean surface of *i*-Ag-In-Yb only the surface features are included in the FFT computation. For further FFT analysis using Cu deposition, all FFT's were filtered also, so that only the Cu clusters not the quasicrystal surface are computed giving a more accurate FFT. Using an STM image, the "hills" i.e. the features of the surface, whether it be clean surface or Cu clusters could be filtered out by choosing to measure the image above a minimum height. Once the correct height was chosen and the image appeared to exhibit the right level of features for that particular study, the FFT was computed.

Due to the special treatment of this sample, the sputter-annealing process produced localisation in the cleaning of the surface. This limited the STM analysis to a small section within the centre of the surface sample thus reduced the range of which the surface could be studied.

To analyse the step height distributions which separate the terraces, the software WSxM was used. Once an image was selected and "flattened", a terrace was highlighted using the "local plane" function and this then generated a new image of the terraces and steps. Selecting the histogram function then produced a plot of the range of heights within the full STM image. The markers on the histogram could be moved in to place to the peaks of the step height distributions and the differences in height would be recorded.

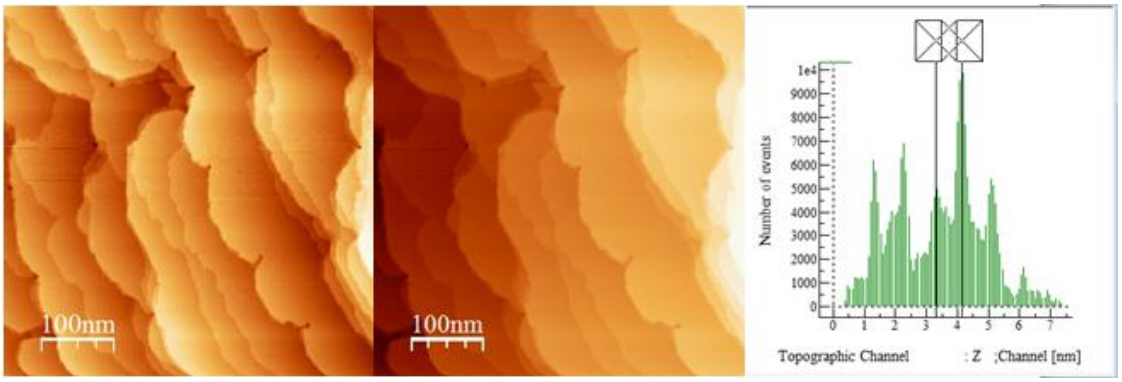

Figure 5-6 Analysis of step height distribution.

103 different heights were recorded this way from 25 different clean surface STM images. To analyse the height distribution of the steps and their occurrence a histogram of averages was plotted of the 103 different heights recorded. The heights were separated in to appropriate bins separated by 0.050 nm steps. The average height within each step was calculated, and then the weighted average of each of the three peaks that were present in the histogram was also calculated.

Height of step (nm)	No. in each bin	Average height in each bin (nm)	Average Height (nm)	Error (nm)
0.100-0.149	1	0.145		
0.150-0.200	4	0.175		
0.200-0.249	18	0.241		
0.250-0.300	27	0.272	**0.289**	0.114
0.300-0.349	8	0.312		
0.350-0.400	8	0.368		
0.400-0.449	3	0.425		
0.450-0.500	4	0.464		
0.500-0.549	0	0		
0.550-0.600	5	0.582		
0.600-0.649	5	0.621	**0.646**	0.065
0.650-0.700	1	0.650		
0.700-0.749	5	0.735		
0.750-0.800	0	0		
0.800-0.849	5	0.835		
0.850-0.900	5	0.864	**0.883**	0.064
0.900-0.949	4	0.917		
0.950-1.000	2	0.981		

Table 1 Weighted distribution of heights.

A histogram of the occurrence of the various step heights was then plotted. The average height of each of the 3 peaks was also placed on the plot to give an indication of the how well the overall data fitted the average. From previous clean surface STM studies on *i*-Ag-In-Yb, over 400

steps shown that the average step heights are close to three values; S = 0.28(±0.04) nm, M = 0.58(±0.03) nm and L = 0.85 (±0.05) nm and their respective occurrence is 66%, 12% and 22% [1].

The data taken from this study of 103 steps, shown the average step heights were found to be; S = 0.289(±0.114) nm, M = 0.646(±0.065) nm and L = 0.883 (±0.064) nm with their respective occurrence being 70%, 15% and 15%. The average step heights are in quite close agreement with the previous results, especially the S and L values. The heights of S = 0.289(±0.114) nm and L = 0.883 (±0.064) nm satisfy the previous values of S = 0.28(±0.04) nm and L = 0.85 (±0.05) nm. It is clear that the occurrences of the M steps are less preferred and it is the S and L steps which are more important. The occurrence percentages of 70%, 15% and 15% in this study don't fully compare to 66%, 12% and 22% in the previous study of four times the amount of the steps that were researched. The frequency of the Large and Medium steps are equal at 15%, however from observation of the clean surface images it is clear that the Medium steps which can be seen in Figure 5-2 are of narrow width. Unlike the Large steps which have formed in much wider terraces, the Medium steps are clearly not as stable during formation as the Large and Small steps. It is possible that the 103 steps investigated here may not be sufficient enough in number to be completely agree with the values found in the more extensive study of 400 steps.

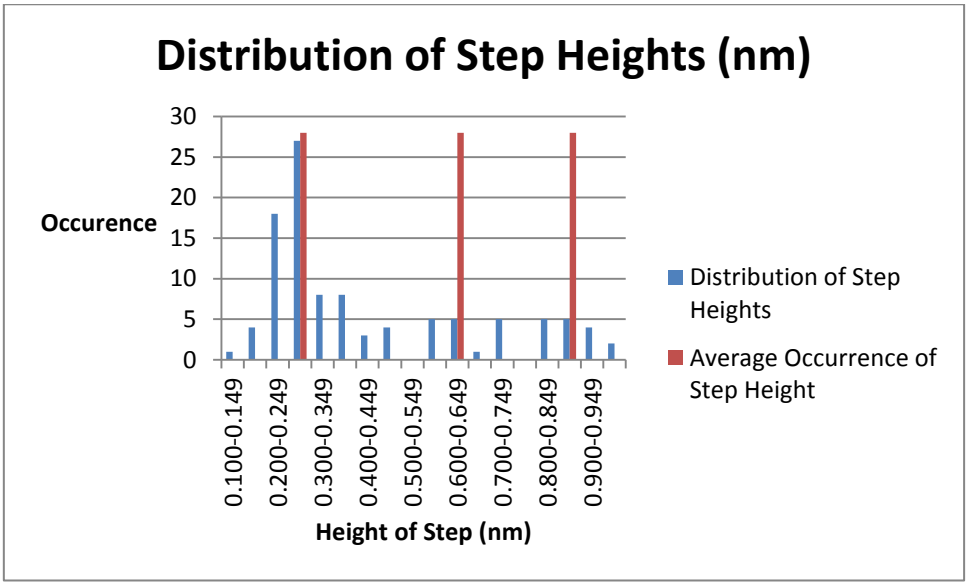

Figure 5-7 Histogram of weighted average occurrence of heights.

Further confirmation of the formation and presence of the steps and terraces on the surface can be seen in Figure 5-8 (500 nm x 500 nm, -1 V) using the line profile used in WSxM;

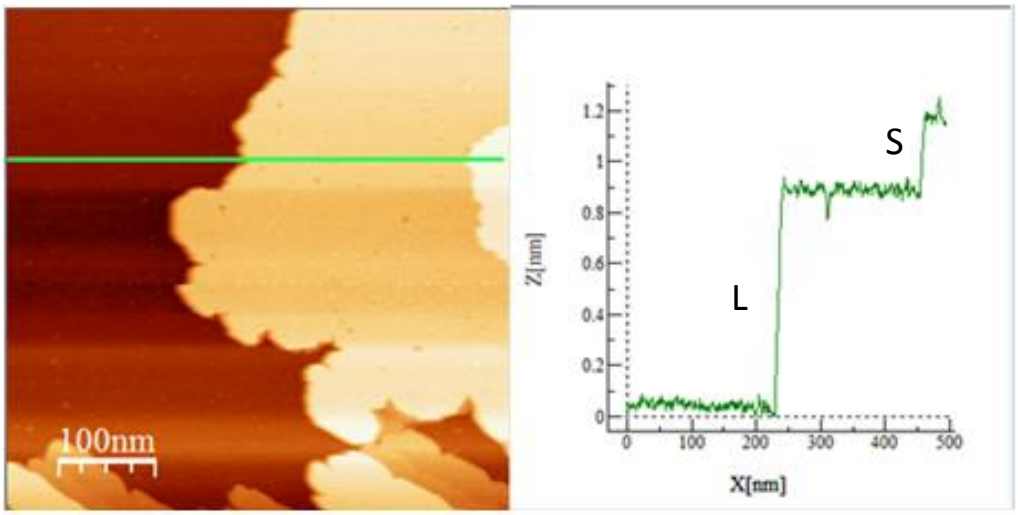

Figure 5-8 Line profile indicating Large and Small terraces.

The Small (S) and Large (L) steps can be clearly seen in the line profile for Figure 5-8. The L step is approximately 3 times larger than the S as expected from the measurements of S = 0.289(±0.114) nm and L = 0.883 (±0.064) nm. These steps correspond to the separation of the bulk planes which intersect the centre of the RTH clusters which make up the *i*-Ag-In-Yb surface [3].

The STM image analysis of the clean surface so far confirms the quasiperiodicity of the *i*-Ag-In-Yb sample. The crystal exhibits quasiperiodic symmetry seen in both real LEED patterns and FFT analysis of the surface. The measurements of the step and terrace morphology have also shown that this particular *i*-Ag-In-Yb crystal compares well to samples from other experiments [1].

5.2 Study of Cu Deposition on *i*-Ag-In-Yb

5.2.1 Low Coverage

To study the deposition of Cu on the *i*-Ag-In-Yb surface, high purity Cu wire was wrapped around a simple Ta filament. A power supply of 3 Amps was applied to the Ta filament and the Cu was deposited by evaporation for 20 seconds, 40 seconds, 1 minute 45 seconds and 1 minute 50 seconds on to the quasicrystal surface. STM images were obtained using the same techniques for the clean surface studies. Over 100 STM images were obtained from various locations on the surface, using both positive and negative bias voltage. Different scales of images varying from 500 nm x 500 nm to 75 nm x 75 nm were able to show the formation of the Cu not only on the larger scale of the terrace but close to the surface, enabling good atomic resolution of the formation of Cu.

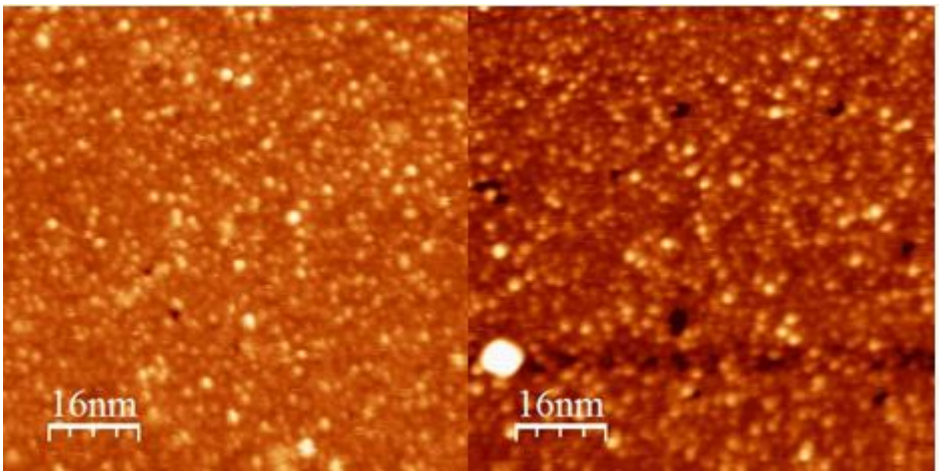

Figure 5-9 Low coverage Cu deposition:

LEFT 20 second deposition, 80 nm x 80 nm, -1.7 V : RIGHT 45 second deposition, 80 nm x 80 nm -2.1 V.

Figure 5-9 shows images from the 20 and 45 second deposition of Cu. The bright spots which appear in both images represent the beginning of the formation of the Cu clusters on the *i*-Ag-In-Yb substrate. The left image (20 secs, 80 nm x 80 nm, -1.7 V) shows many bright spots on the substrate quite consistently spread out. The second image (45 secs, 80 nm x 80 nm, -2.1 V) at twice the deposition time shows a similar distribution of Cu clusters beginning to form on the surface. Both images show good atomic resolution.

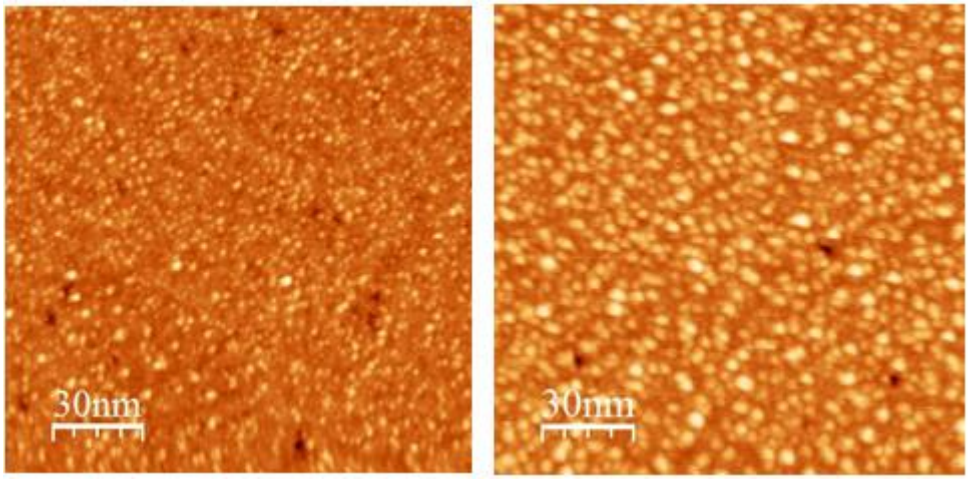

Figure 5-10 Low coverage Cu deposition:

LEFT 1 minute 45 second depostion, 150 nm x 150 nm, +1.3 V : 1 minute 50 second deposition, 150 nm x 150 nm, -1.2 V.

Figure 5-10 continues to show an increase in Cu cluster formation. The left image (1 min 45 secs, 150 nm x 150 nm, +1.3 V) shows a large but evenly distributed spread of bright spots which indicate the Cu atoms present on the surface. The image on the right (1 min 50 secs, 150 nm x 150 nm, -1.2 V) shows large uniform clusters forming quite frequently across the surface.

STM images which are at negative bias voltage are characterised by large Ag & In protrusions, some of which are arranged in pentagons. The positive bias images however display Yb rings, which appear at the vertices of the pentagons. Due to the coverage after 1 minute 50 second deposition being relatively low, the substrate structure can still be seen clearly. Figure 5-11 and Figure 5-13 shows the expected pentagons and rings which are characteristic of the quasicrystal surface [1].

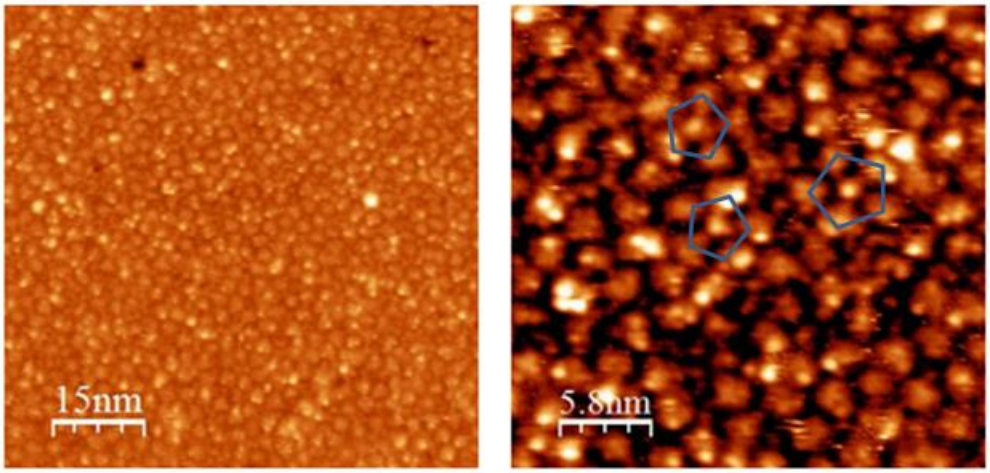

Figure 5-11 - 1 minute 50 second deposition, negative bias:

LEFT 75 nm x 75 nm, -1.2 V STM image showing detailed surface structure at negative bias

RIGHT 29 nm x 29 nm, -1.2 V STM image exhibiting Ag-In protusions forming pentagons.

Figure 5-11 shows the 1 min 50 second deposition at -1.2 V next to an enlarged section of the image. The image on the right shows some of the protrusions of the *i*-Ag-In-Yb surface forming pentagonal shapes. The adsorption of the Cu atoms can also be seen throughout the image, not only on the pentagons but the protrusions in general. The pentagon's seen here are the first real space images of the sample used in this study that suggest five-fold symmetry. To confirm that the surface possesses such symmetry, another FFT was computed after filtering;

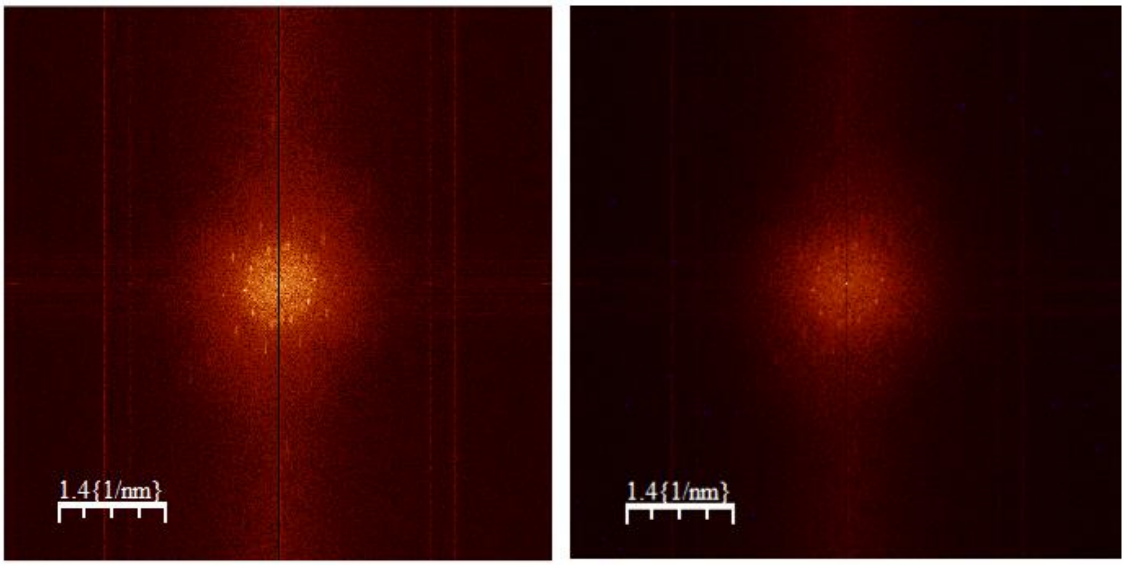

Figure 5-12: FFT images of Figure 5-11 showing two rings of ten spots indicating quasiperiodic symmetry at negative bias.

LEFT: Unfiltered FFT of surface

RIGHT: FFT image of filtered Cu substrate only.

The inner and outer rings of 10 spots, confirm the forbidden quasicrystal symmetry. The filtered FFT of the substrate showing that the STM image after low Cu deposition possesses quasiperiodic symmetry is the first suggestion that Cu may begin to form in a quasicrystalline aperiodic order on the surface of *i*-Ag-In-Yb.

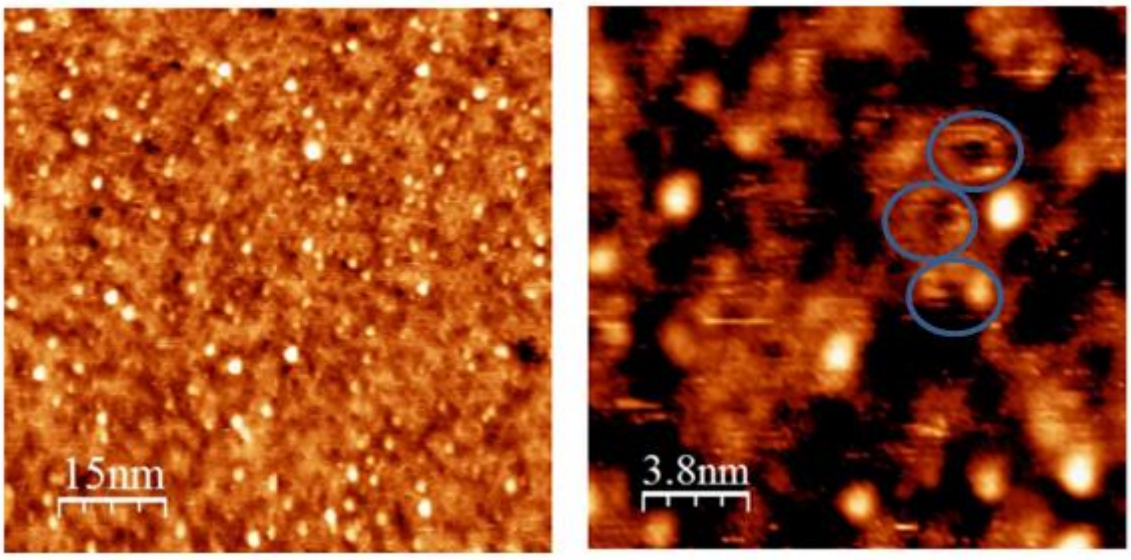

Figure 5-13 1 minute 50 second deposition, positive bias:

LEFT 75 nm x 75 nm, +1.2 V STM image showing detailed surface structure at positive bias

RIGHT 19 nm x 19 nm, +1.2 V STM image exhibiting Yb rings.

Figure 5-13: the image on the left (1 min 50 sec, 75 nm x 75 nm, +1.2 V), obtained using positive bias voltage is characterised by the expected Yb rings at the vertices of the pentagons. The resolution at positive bias isn't as clear as the images obtained at negative bias, however the image on the right does appear to show a few clusters of rings.

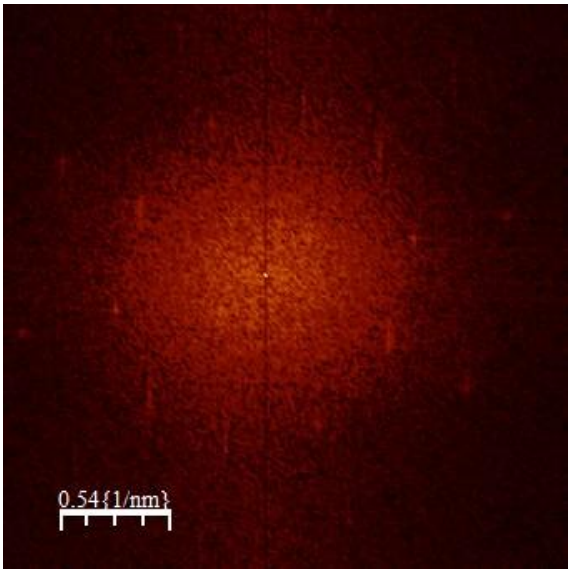

Figure 5-14: FFT image of Figure 5-13 at positive bias exhibiting forbidden symmetry.

An FFT of the filtered Cu substrate shown in Figure 5-14 in shows the same symmetry present in the FFT of the surface taken shown left in Figure 5-12 at negative bias voltage.

The next step in the study of the low coverage Cu deposition was to measure the characteristic protrusions and rings. This would again confirm that the *i*-Ag-In-Yb sample being used for this study possesses the same structural properties from that of other studies. In previous studies the pentagons have been measured as having an edge length of 2.40(±0.15) nm, and the diameter of the protrusions were measured to be 1.30(±0.04) nm. The diameter of the rings using a positive bias is 1.80(±0.05) nm [1].

The measurements of the pentagon edge lengths were obtained using a line profile where the distance in the lateral x-direction was measured.

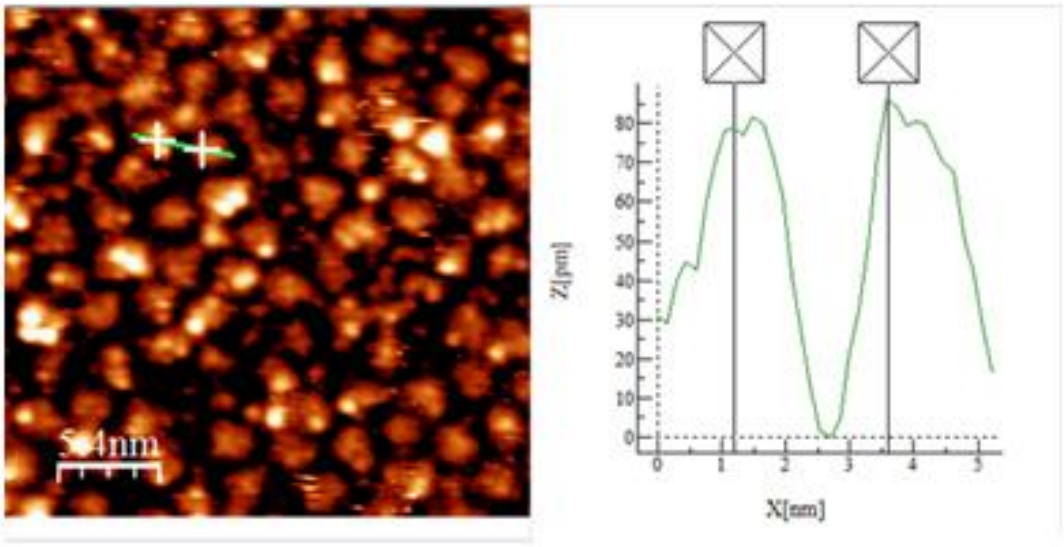

Figure 5-15 Line profile showing measurement of Ag-In protrusion seperation.

A pentagon edge length was chosen, and then a line profile was selected and placed across two protrusions. The markers were then placed at the peaks of the height of the protrusions, and the distance in the x direction between the markers was recorded as the protrusion separation. Approximately 100 edge lengths were measured from the 1 min 50 secs, 75 nm x 75 nm, -1.2 V STM image using this method. The average pentagon edge length was found to be 2.42(±0.18) nm. This value matches the previously measured value of 2.40(±0.15) nm excellently [1].

The diameter of the protrusions which make up the pentagons was estimated using the full width half maxima of the height profiles.

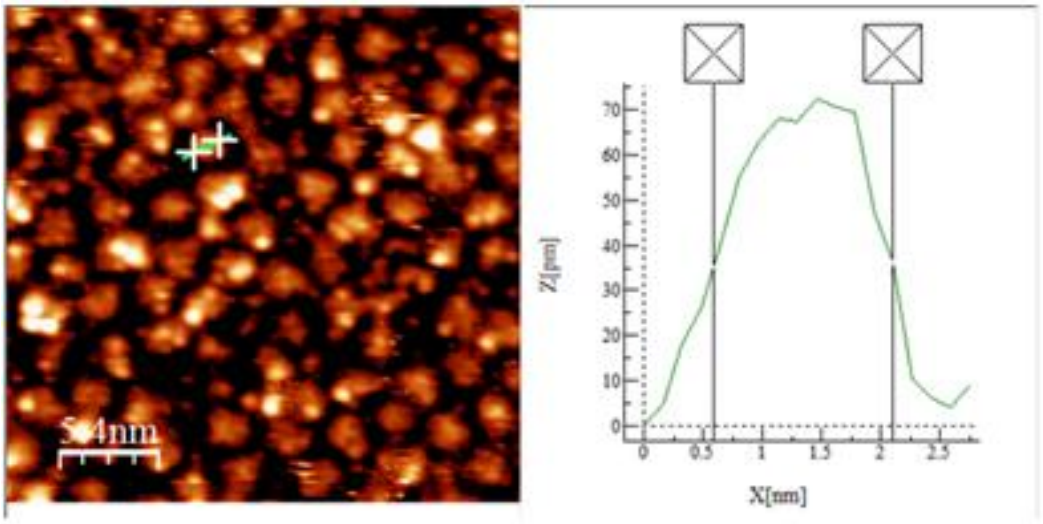

Figure 5-16 Line profile using FWHM estimation to measure protrusion height.

Each protrusion which formed a pentagon was selected using the line profile tool. The markers were then placed at an estimation of half the maximum height of the peak. The distance in the

x direction between the markers was recorded as the diameter of the protrusion. The average diameter was found to be 1.32(±0.11) nm. The value of 1.30(±0.04) nm obtained in [1], shows that the value from this study is an extremely good match, confirming that the protrusions studied are comparable to those previously studied. The building blocks which make up the *i*-Ag-In-Yb RTH cluster are represented in Figure 5-17. The terraces formed on the surface are the planes which intersect the rhombic tricontahedral shape perpendicular to the five-fold axes seen in Figure 5-17. The Icosidodecahedron has a radius of 0.65 nm radius and therefore has a diameter of 1.30 nm. The protrusion diameter measurement of 1.32(±0.11) nm is an accurate measurement of the Ag-In Icosisdodecahedron which makes up the RTH clusters.

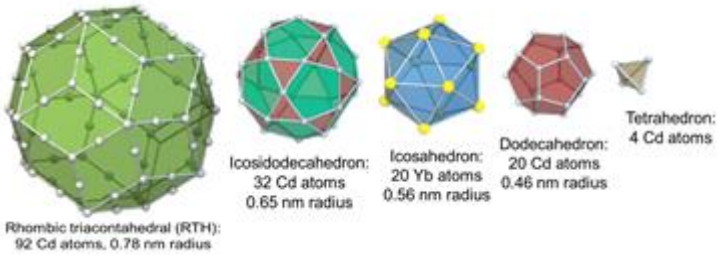

Figure 5-17 Building blocks of *i*-Cd-Yb.

Using a positive bias voltage, the Yb rings seen in Figure 5-13 were able to be measured using the line profile, and putting the markers in to place;

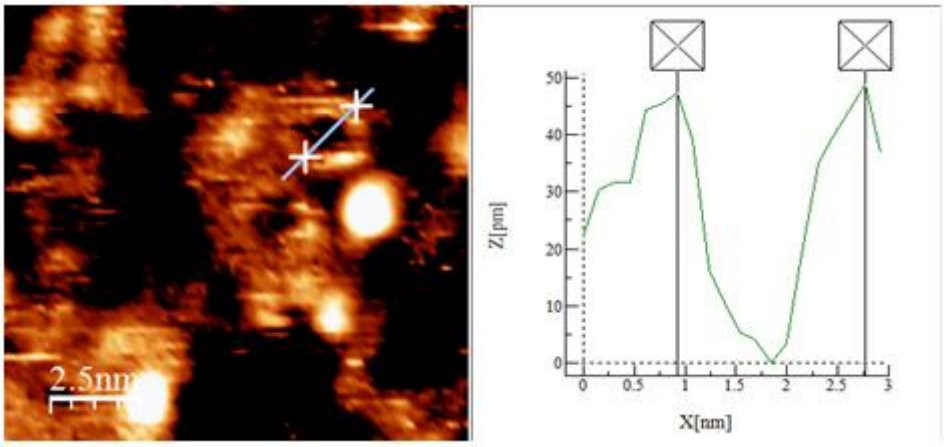

Figure 5-18 Line profile showing measurement of Yb ring diameter.

Just as the pentagon edge lengths and the protrusion diameters in this study matched the values from previous studies, the average ring diameter measured was 1.76(±0.14) nm and shows close agreement to the existing value of 1.80(±0.05) nm.

To analyse the adsorption structure of Cu on the *i*-Ag-In-Yb surface, the height and lateral size of the Cu clusters which can be seen on the protrusions in the STM image in Figure 5-11 were also measured. The purpose of measuring the height and the diameter of the Cu atoms is to determine the preferred growth mode. Certain values of height and lateral size will provide an insight as to whether the Cu forms in a layer by layer growth method or possibly by 3-D growth. The presence of Cu clusters is represented by bright spots on the surface of the protrusions and all deposition times were considered when measuring the dimensions of the Cu on the substrate surface.

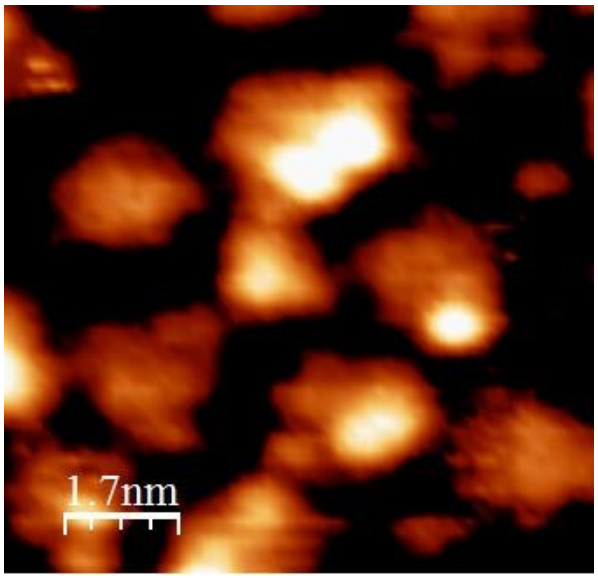

Figure 5-19 Enlarged image of Figure-11, 8.5 nm x 8.5 nm, -1.2 V, exhibiting Cu clusters forming on Ag-In protrusions.

The Cu clusters can clearly be seen in Figure 5-19 on the surface of the protrusions. The measurements of the lateral size of the Cu atoms were obtained using the same line profile methods as done before for the protrusion diameter using the FWHM estimation. The height of the Cu atoms on the surface of the protrusion were determined using the line profile and placing one marker on the peak of the distribution representing the full height of the Cu atoms and placing the last marker at a minimum on the line profile;

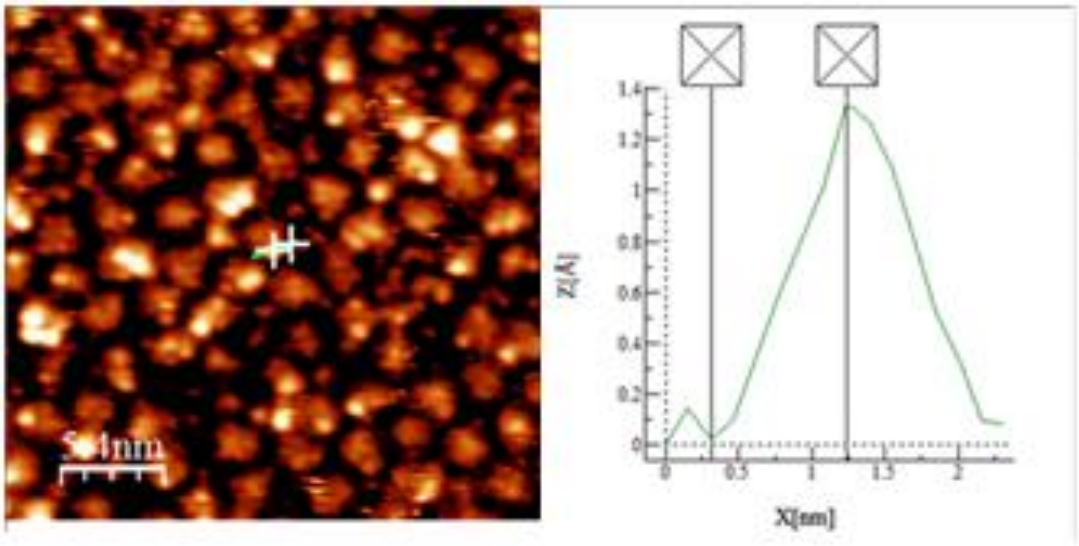

Figure 5-20 Line profile showing measurement of Cu cluster height on Ag-In protrusions.

After measuring over 100 Cu atoms after 1 minute 50 second deposition at a resolution of 75 nm x 75 nm the average height from the data recorded this way was found to be 1.29(±0.13) Å.

The size of the same number of Cu atoms was measured in the same way as the Ag-In protrusions, using the FWHM estimation method;

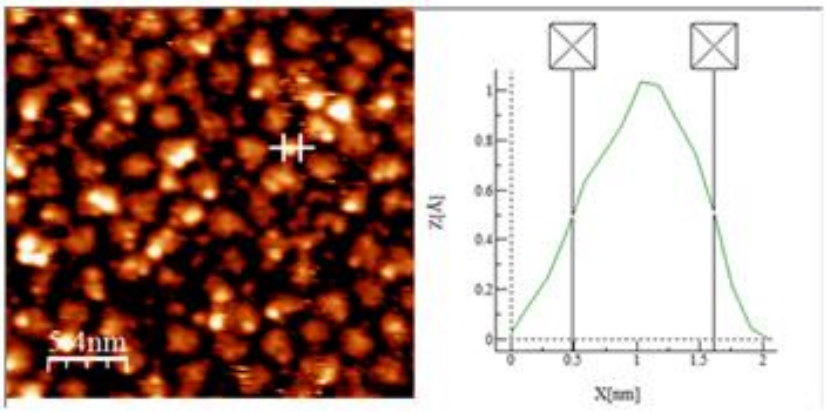

Figure 5-21 Line profile showing Cu cluster size measurement using FWHM estimation.

The average lateral size of the Cu clusters in nm was found to be 1.21(±0.23) nm.

The values of 1.29(±0.13) Å for height and 1.21(±0.23) nm lateral size suggest that the Cu atoms have formed a layer which spreads in the lateral direction. This is confirmed by the height of the Cu clusters being almost exact to the true radius of a Cu atom. The lateral size of the clusters is a factor of 10 larger than the height suggesting a flat layer is beginning to form, consisting of Cu atomic clusters. It is worth nothing that the measurements of height were obtained using a high resolution of 75 nm x 75 nm for this particular measurement. The later comparison of heights in relationship to coverage and deposition time was taken from images of 150 nm x 150 nm resolution.

Studying the preferred adsorption positions of the Cu clusters at both positive and negative bias voltages is important in the understanding of the adsorption structure of Cu. Changing the bias voltage enables different aspects of the quasicrystal surface to be seen, with negative bias showing the Ag-In pentagonal protrusions, whilst positive bias gives insight to the Yb rings formed at the vertices of these pentagons.

A simple quasicrystal model of the surface terminating bulk plane demonstrates where the pentagons should exist in relation to the structural rings [1].

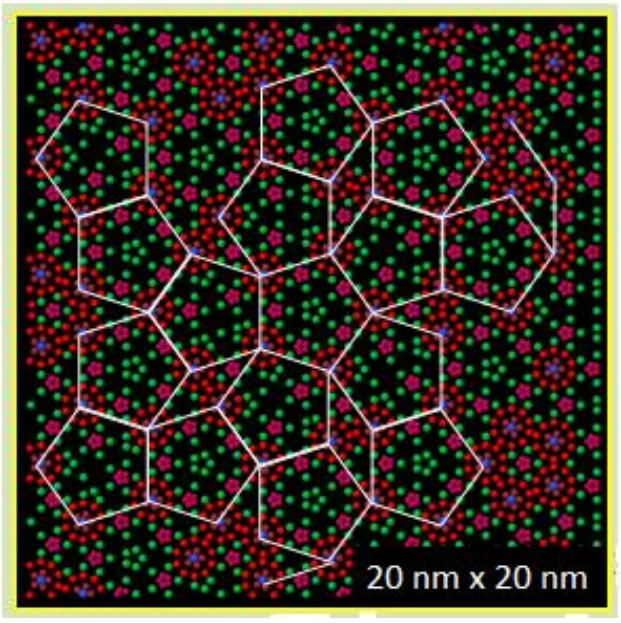

Figure 5-22 Quasicrystal model of surface terminating bulk plane [9]

Figure 5-22 shows a Penrose tiling on the surface of the predicted atomic model for the quasicrystal structure. The Penrose tiling overlays perfectly on to the structure of the model rings, with the vertices of the pentagons at the centre of these rings. The Ag-In protrusion pentagons are compiled of the blue spots seen on Figure 5-22 and the Yb rings are displayed by the red rings at the vertices of these pentagons.

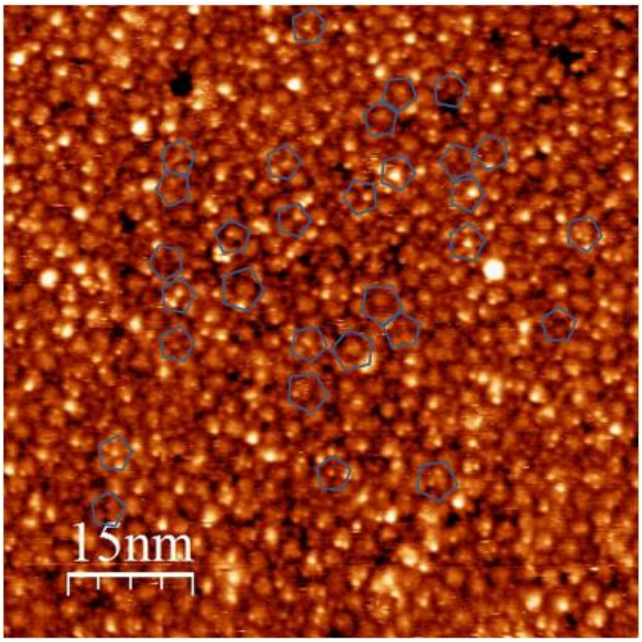

Figure 5-23 Overlaying of pentagons on negative bias STM image showing start of Penrose tiling build up

Similar to the Penrose tiling layered over the quasicrystal model in Figure 5-232, Figure 5-23 (1 min 50 sec, 75 nm x 75 nm, -1.2 V) has pentagonal shapes over layed on to the positions of the pentagonally arranged protrusions. The majority of the Cu clusters appear to exist at the vertices of the pentagons although a minority can be found on the protrusion in the centre of the pentagon. The clusters tend to completely cover a large part of the surface area of the protrusion if not all. In the model it can be seen that the blue spots are placed exactly on the corners of the pentagons, therefore Figure 5-23 shows good agreement with the quasicrystal model and the beginning of a Penrose tiling can be seen to build up. From the model it can also be deduced that the red rings from the quasicrystal model form in pentagons.

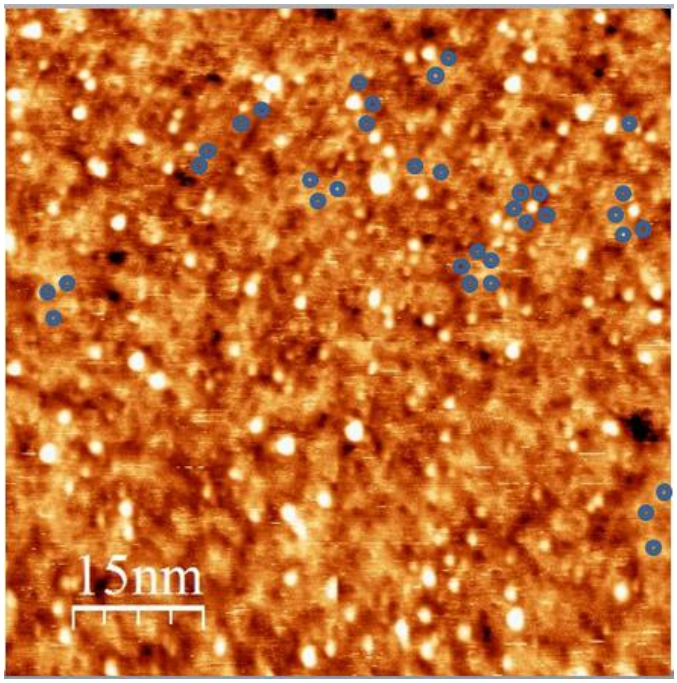

Figure 5-24 Over layered circles placed on the Yb rings seen on positive bias STM image

Figure 5-24 (1 min 50 sec, 75 nm x 75 nm, +1.2 V), displays blue rings layered on top of the Yb rings found on the STM image. The image shows that the rings that are seen on the image do form in pentagons like the red rings in quasicrystal model. Some of the Cu clusters are found to adsorb directly in the centre of the pentagon displayed by the rings.

Using the same filtering method for the substrate FFT analysis, the "hills" on the surface which represent the Copper clusters can be singled out and the average distance between nearest neighbouring clusters can be obtained. These are the average values of the separation of the Cu clusters at low coverage

- 2.77 nm separation after 20 seconds
- 2.38 nm separation after 45 seconds
- 2.02 nm separation after 1 minute 50 seconds

These values are relatively close to the Ag-In protrusion separation measurements from the clean surface (pentagon edge length) of 2.42(±0.18) nm which suggests that the Cu clusters prefer to form on the centre of the Ag-In protrusions.

5.2.2 High Coverage

To study the deposition of Cu on the *i*-Ag-In-Yb surface at high coverage the same power supply of 3 Amps supplied to the filament and the Cu was deposited by evaporation for 4, 10 and 16 minutes on to the quasicrystal surface. Over 100 STM images were obtained from various locations on the surface, using both positive and negative bias voltage. Different scales of images varying from 500 nm x 500 nm to 75 nm x 75 nm were able to show the increased formation of the Cu atomic clusters that had adsorbed on the surface of the *i*-Ag-In-Yb. Measurements of the heights and lateral sizes of the clusters formed on the substrate surface would give insight in to the growth mode of the Cu, and how it differs from the behaviour at lower coverage.

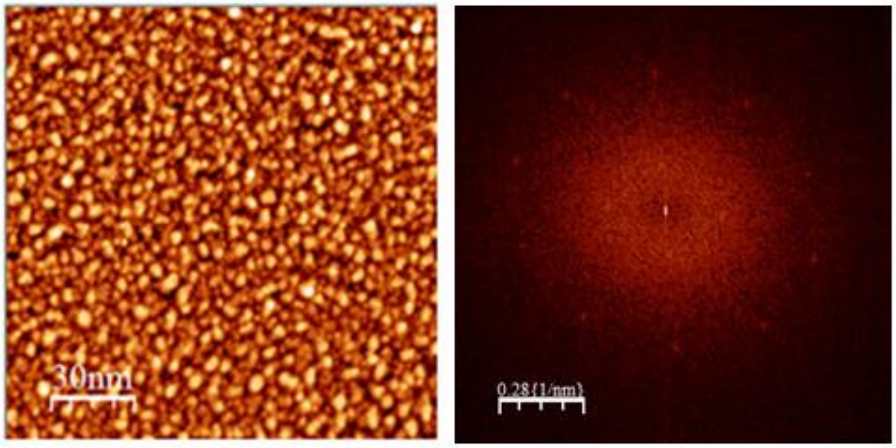

Figure 5-25 High Cu coverage, 4 minute deposition:

LEFT 150 nm x 150 nm, -1 V, showing increase build up of Cu formation:

RIGHT FFT image of surface exhibiting quasiperiodic symmetry.

Figure 5-25 was obtained after a 4 minute deposition of Cu at 150 nm x 150 nm resolution using an applied bias voltage of -1 V. The STM image on the left shows an increased build of Cu atoms on the surface of the substrate compared to the previous images at low coverage. The filtered FFT image indicates that the Cu substrate still possesses quasiperiodic symmetry even at high coverage. The STM image shows good resolution of the surface however the substrate protrusions cannot be seen in the images due to the Cu forming completely over the substrate surface. To confirm this, a line profile was performed on the clean surface images and the low coverage images and shown the protrusion height to always be lower than a height of approximately 1.3 Å. In Figure 5-25 only Cu formation can be seen, this was confirmed by a line profile of the complete surface which only had peaks of height greater than 1.3 Å, suggesting that all the substrate protrusions had been completely covered by Cu clusters.

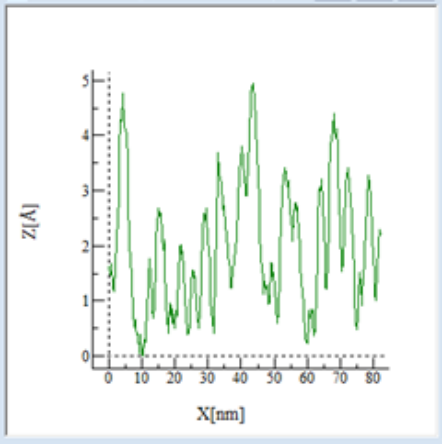

Figure 5-26 Line profile showing height of Cu on *i*-Ag-In-Yb.

Figure 5-26 shows height profile of the STM image from Figure 5-25

It is clear from Figure 5-25 that the Cu atoms continue to form clusters at an increased coverage. The complete quasicrystal surface has been covered by the single element over-layer. The clusters throughout the image at 4 min deposition appear to be less uniform than clusters seen in the 1min 50 second deposition of Cu. This suggests that individual Cu atoms may have some preferred absorption site a lower coverage due to individual atoms potentially diffusing over the surface. The height and lateral sizes of the Cu clusters at 4min deposition were measured using the same techniques used for the data at lower coverage. Due to the increased Cu coverage, the Copper atoms have formed in clusters of larger width than that of lower coverage and have also formed multiple layers of Cu. This is the first indication that at higher coverage the Cu clusters prefer to form in 3-D islands rather than layer by layer. This is suggest a strong Cu-Cu adsorbate interaction which leads to 3-D growth.

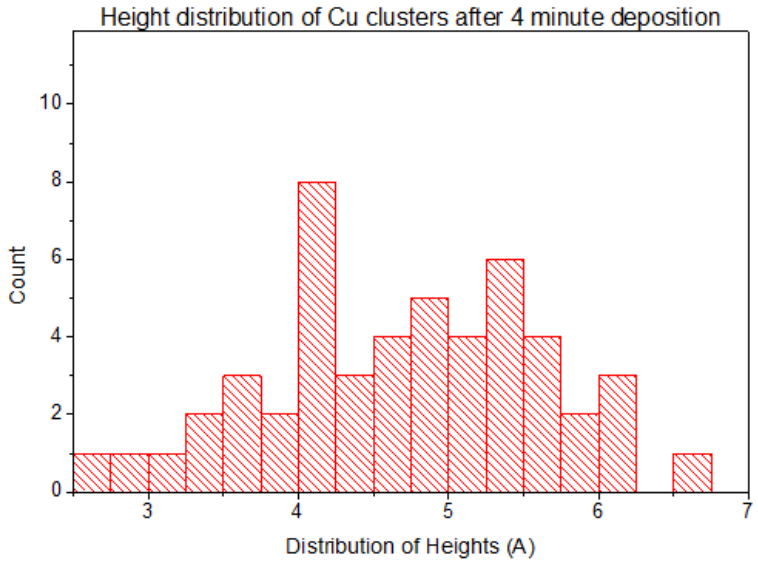

Figure 5-27 Height distribution of Cu clusters after 4 minutes deposition.

Further investigation in to the growth modes of Cu on the surface of the *i*-Ag-In-Yb sample prompted the use of even higher coverage's using deposition times of 10 and 16 minutes.

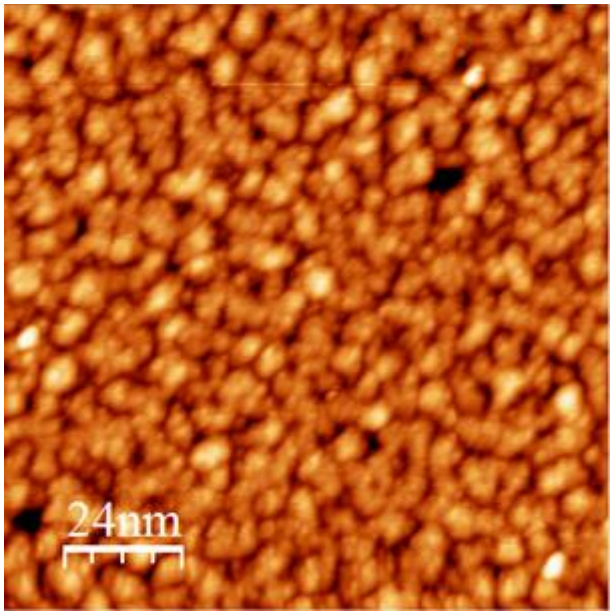

Figure 5-28 High Cu coverage 10 minute deposition, 120 nm x 120 nm, -1.1 V showing further Cu formation.

Figure 5-288 shows an STM image taken at 10 minute deposition at 120 nm x 120 nm using -1.1 V. At more than twice the deposition rate than the previous 4 minute images analysed, it is clear that the clusters appear to become more irregular in shape with an increase in Cu deposition. Due to the deformation away from the previously seen circular clusters at lower coverage, the measurement of the lateral size at 10 minute coverage is difficult to determine due to the irregularity of a constant lateral size in the clusters.

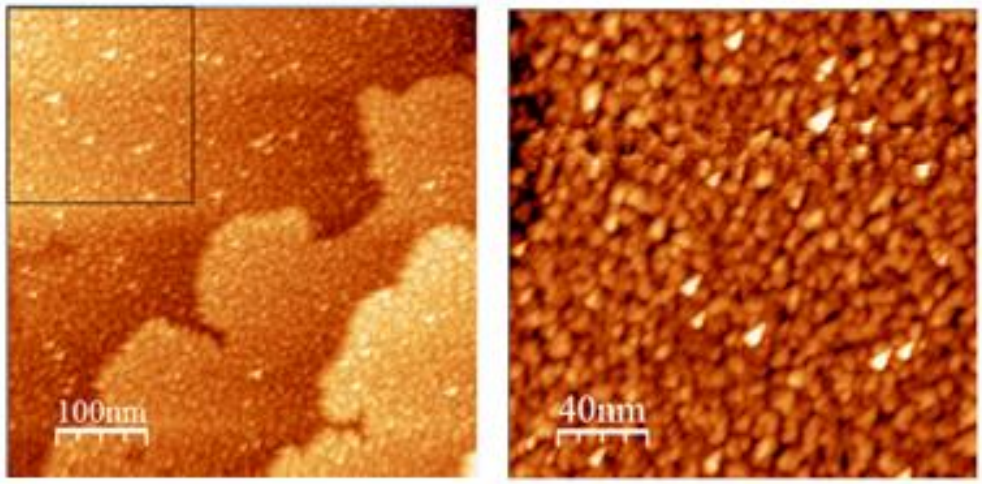

Figure 5-29 High Cu coverage 16 minute deposition, +1.1 V:

LEFT showing further Cu formation 500 nm x 500 nm

RIGHT 200 nm x 200 nm exhibiting large Cu clusters at a more irregular shape.

At coverage of 16 minutes deposition time, the Cu clusters have formed enough to be seen from the image on the left at 500 nm x 500 nm resolution using 1.1 V. The arrangement of the Cu clusters seen in the image on the right of Figure 5-299 at a resolution of 200 x 200 nm can still be found in the highlighted square on the left, indicating how well defined the Cu clusters have formed. Similar to the 10 minute Cu deposition the shapes of the clusters have tended even further away from uniform shape and remain irregular, making the lateral size of the clusters inconsistent to measure.

FFT patterns produced at 10 minute and 16 minute deposition time do not produce forbidden symmetries as seen in Figure 5-4 and Figure 5-25 (clean surface *i*-Ag-In-Yb FFT and 4 minute deposition FFT respectively). Above certain coverage the surface does not exhibit any more quasicrystalline order.

The 10 minute and 16 minute deposition images give even stronger indication that 3-D islands begin to form after certain coverage. It is clear from Figure 5-299 that a flat layer cannot be seen and that irregular shaped islands of different height are present on the surface.

Deposition time (s)	Coverage (ML)	Average Height (A)	Error (A)	Average Lateral Size (nm)	Error (nm)
20	0.19	1.33	0.16	1.67	0.20
45	0.28	1.60	0.22	1.75	0.23
110	0.51	1.99	0.27	3.05	0.32
240	0.93	4.68	0.88	3.86	0.62
600	2-4	5.51	0.91	-	-
960	4-6	7.70	1.77	-	-

Table 2: Table showing the relationship between Cu deposition time and the average size and average height of the Cu clusters.

After complete analysis of the Cu clusters from all the deposition times used, Table 2 gives a summary of cluster parameters in relation to the Cu coverage.

It is to be noted that the calculated average heights do not carry much information in to the formation of the Cu and have only been calculated to show the rate of increase in roughness of the surface compared to the lateral size.

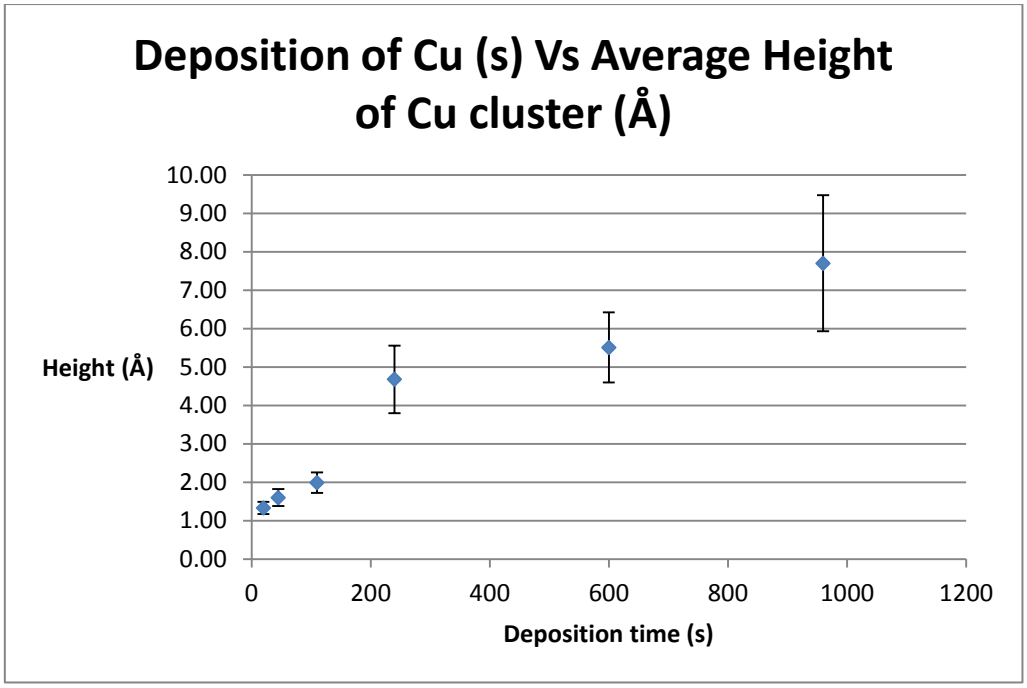

Figure 5-30 Relationship between Cu deposition and increase in average Cu cluster height.

Figure 5-3030 shows the relationship between the increasing Cu depositions against the average heights recorded for each coverage. It is clear from the plot that there is a fairly linear relationship between the increase in Cu deposited and the build-up in height as a result of this. However from the graph it can be seen that there is a clear jump in height from the 1 minute 50 second deposition to the 4 minute deposition. At certain coverage the Cu prefers to form 3-D islands increasing the overall height of the clusters rather than layer by layer growth. As seen in the Volmer-Weber growth mode, a new layer begins to grow before the completion of the last layer. It seems that at a certain coverage the adatom-adatom interaction is greater than that between the adatom and the surface resulting in the Cu atoms preferring to attach to other Cu atoms already formed on the surface, enabling 3-D island growth.

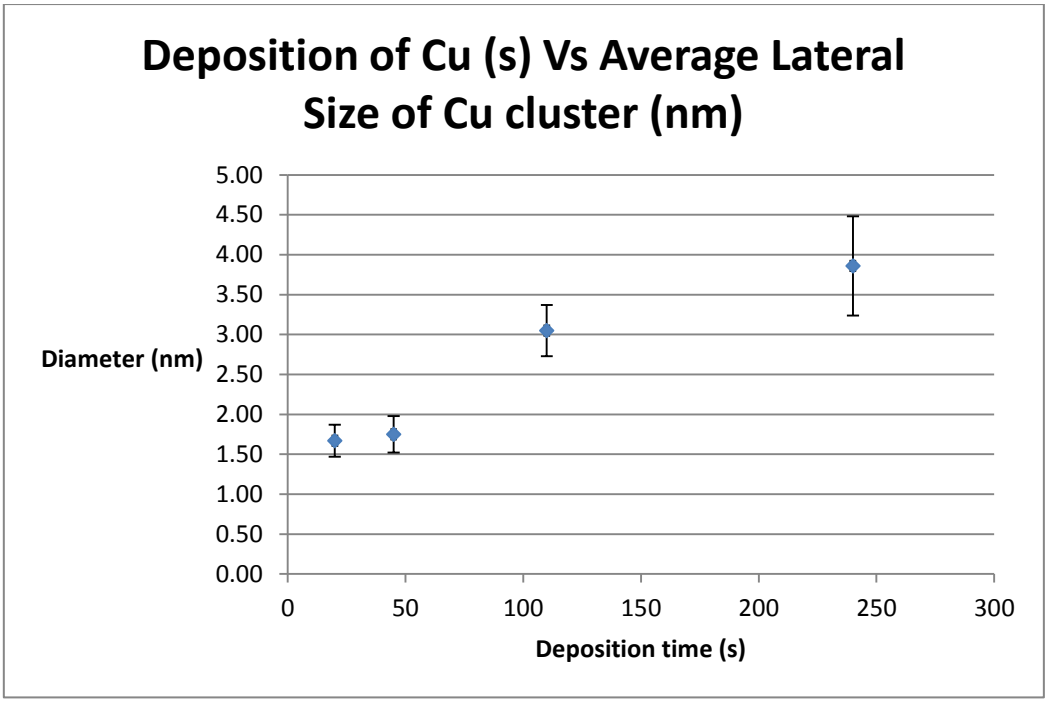

Figure 5-31 Relationship between Cu deposition increase in Cu cluster lateral size.

Figure 5-311 shows the relationship between the Cu deposition rate and the increasing Cu cluster lateral size. Similar to Figure 5-30, there appears to be quite a linear relationship between the lateral size and the addition of the Copper. The 3-D islands not only appear to grow in height but also in lateral lateral size under increased deposition. It appears that the height however increases faster than the lateral size of the clusters. Between 1 minute 50 seconds deposition and 4 minutes, the height increases from 1.99(±0.27) Å to 4.68(±0.88) Å which is an increase of almost a factor of 2.5. The lateral size however increased from 3.05(±0.32) Å to 3.86(±0.62) Å which is only increased by a factor of 1.27. The height increases at a faster rate than the lateral size of the Clusters and this once again confirms the strong interaction of the Cu towards Cu atoms, resulting in the favoured 3-D island growth. It is to be noted that the higher coverage times of 10 minutes and 16 minutes proved difficult for lateral size measurements due to the irregular oblate shape under increased deposition making the choice of which lateral size to measure an unfair representation of the Cu clusters actual size. This is why they have not been included in Figure 5-311.

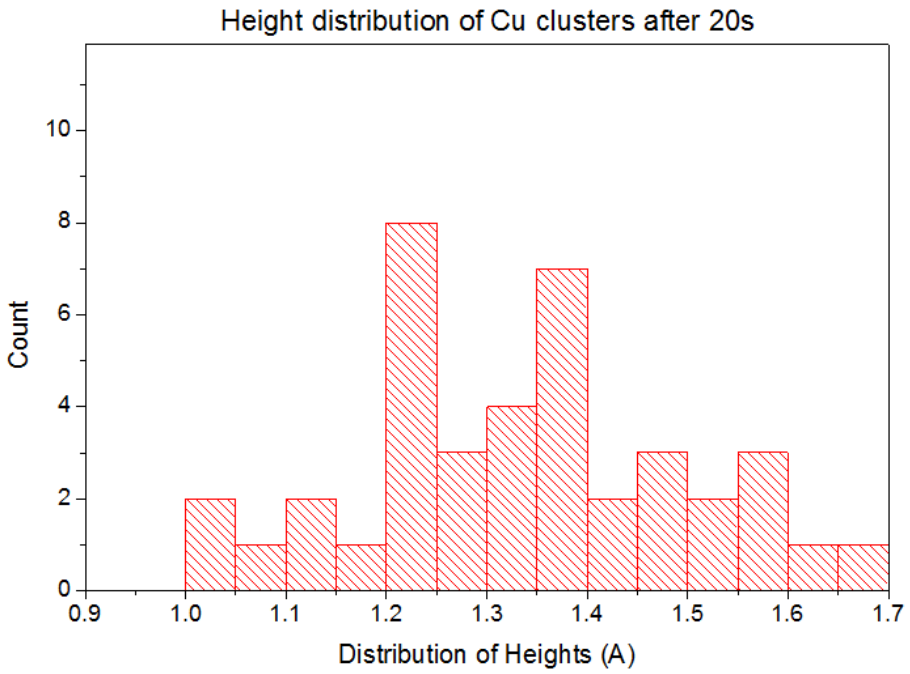

Figure 5-32 Height distribution of Cu clusters after 20 second deposition.

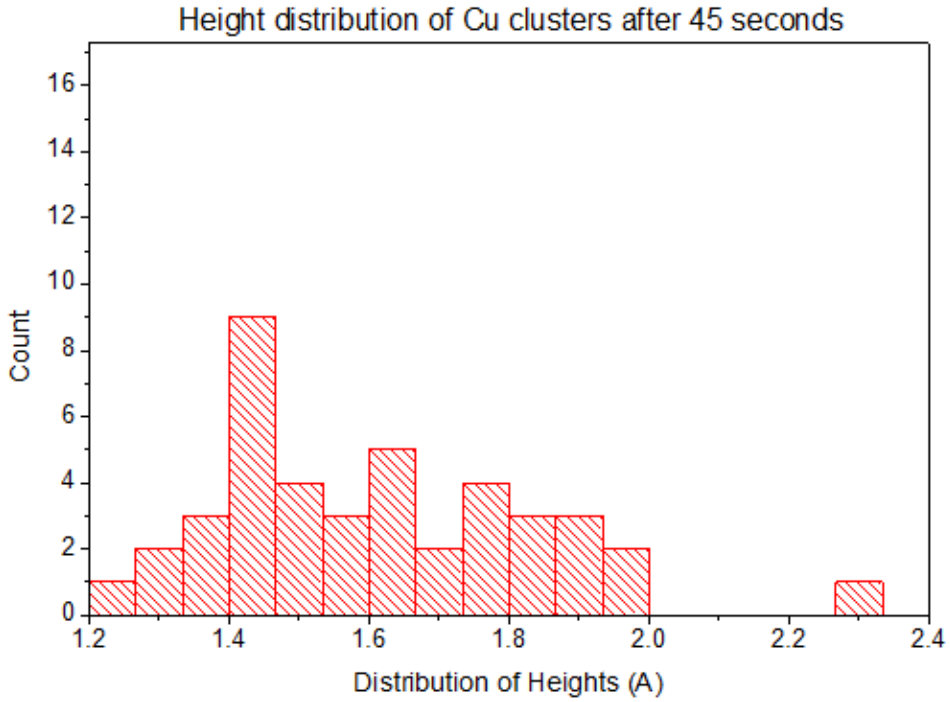

Figure 5-33 Height distribution of Cu clusters after 45 seconds deposition.

Figure 5-32 and Figure 5-33 shows that a large proportion of the heights have the larger occurrence existing between 1.2-1.4Å. This agrees with the expected height value of 1.28Å (Cu

radius) at low coverage. The histogram shows at this low coverage of Cu deposition that a preferred height value of around 1.3Å is present, indicating that a single layer of Copper is beginning to form.

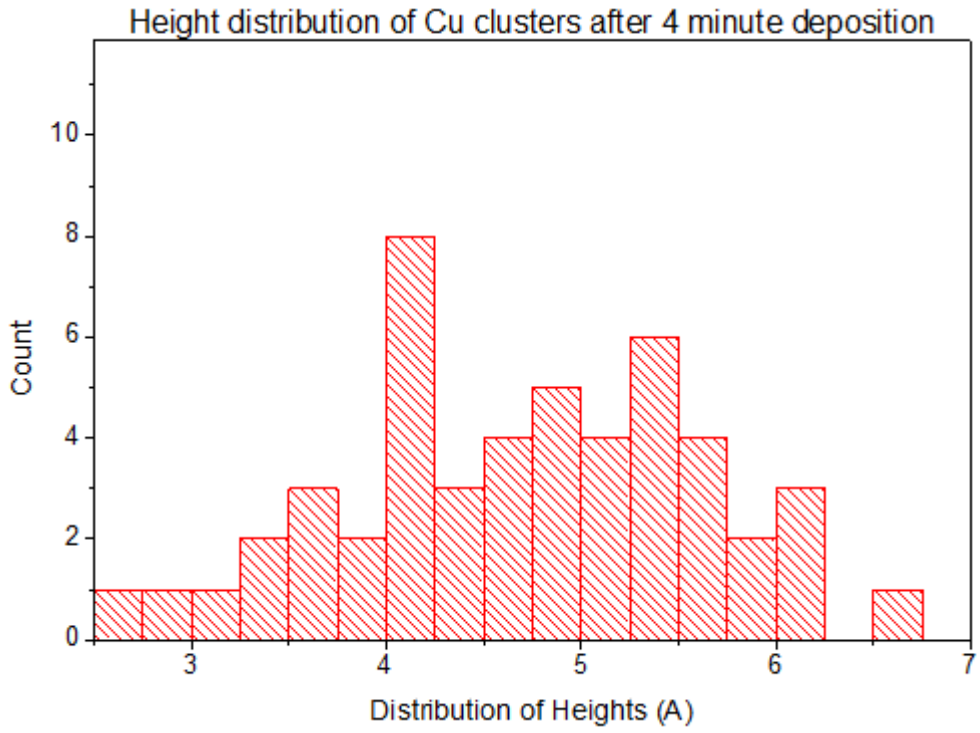

Figure 5-34 Height distribution of Cu clusters after 4 minute deposition.

Figure 5-344 at 4 minute deposition displays that a larger number of various height occur, than at lower coverage. This suggests that there isn't a preferred height after certain coverage and that the clusters become more 3-D at this higher coverage. The clusters appear to be less "flat" and begin to develop in to a more 3-Dimenstional shape. A similar comparison to the lateral size of the Clusters after 20 second and 4 minute deposition also suggests this;

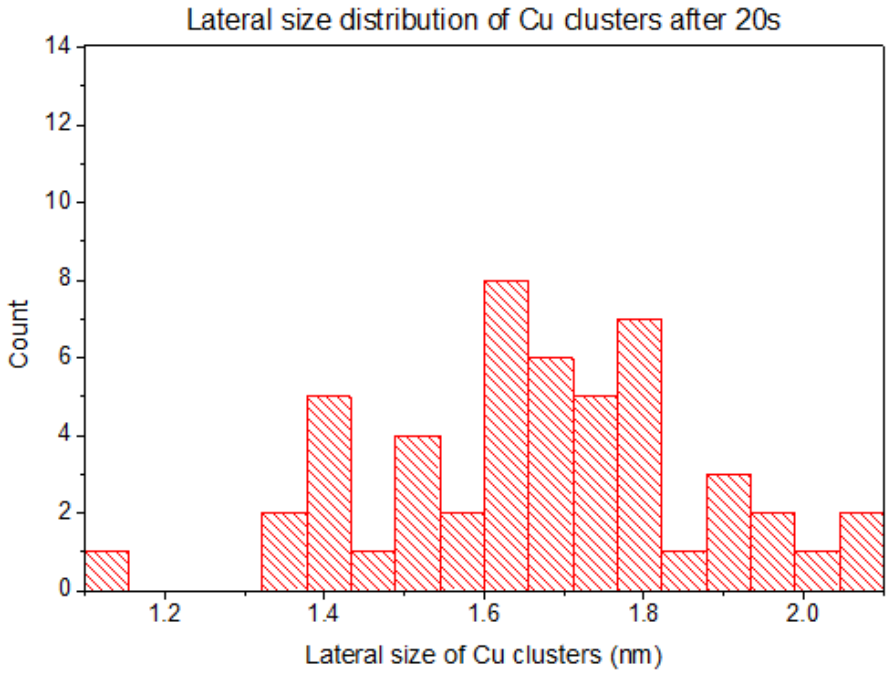

Figure 5-35 Lateral size distribution of Cu clusters after 20 second deposition.

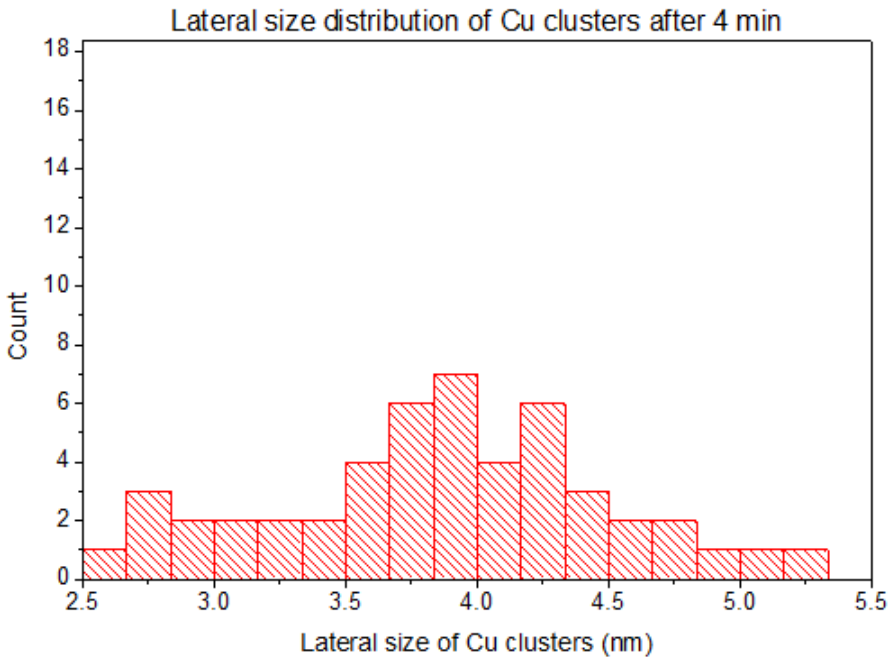

Figure 5-36 Lateral size distribution of Cu clusters after 4 minute deposition.

Figure 5-365 and Figure 5-366 show similar distributions to that of the height comparisons at the same deposition times. At lower coverage where the clusters are more circular and consistent in size, Figure 5-355 reflects this by containing most of the data at a certain point. However at a higher coverage the STM images suggested that the Clusters become more irregular in shape with an increased in Cu deposition. Figure 5-366, like Figure 5-344 displayed a larger variety of lateral sizes present, indicating that there is a tendency away from a preferred shape or size. This again further proves the theory that 3-D islands start to form after certain coverage.

A histogram was plotted using the height data taken for the 16 minute Cu deposition. As previously stated, the lateral size at such a high coverage proved difficult to measure precisely.

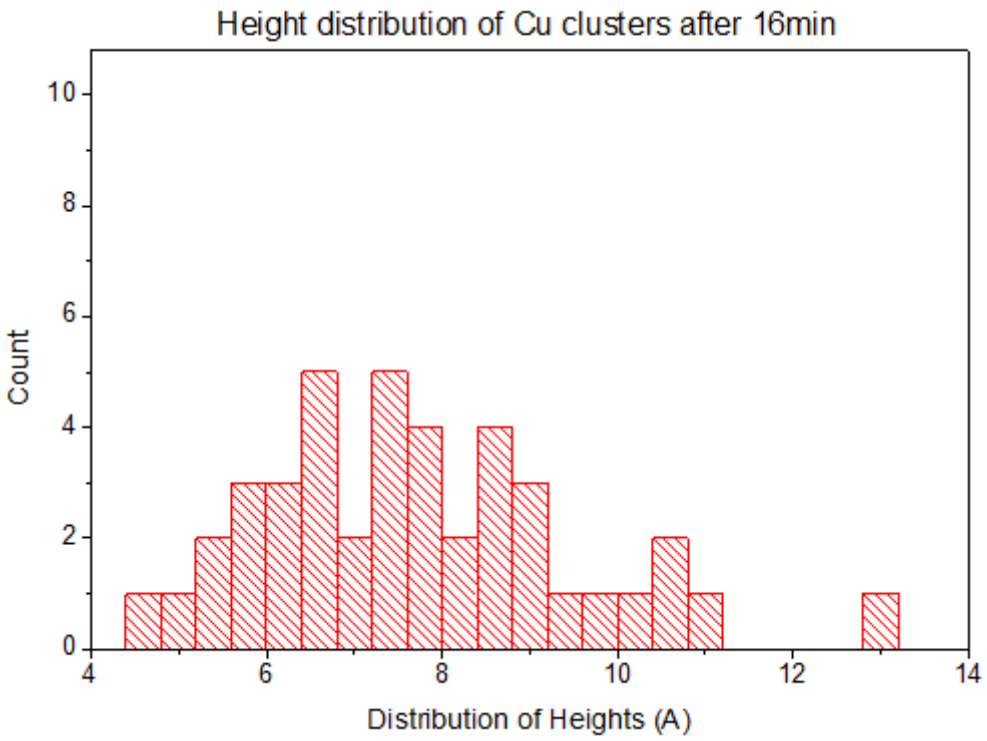

Figure 5-37 Histogram distribution of Cu clusters after 16 minute deposition.

Figure 5-377 continues to show that a variety of heights are present with large occurrence. The majority of the heights occur between 5-9Å meaning that there is no preferred height with multiple 3-D islands of various heights existing on the surface.

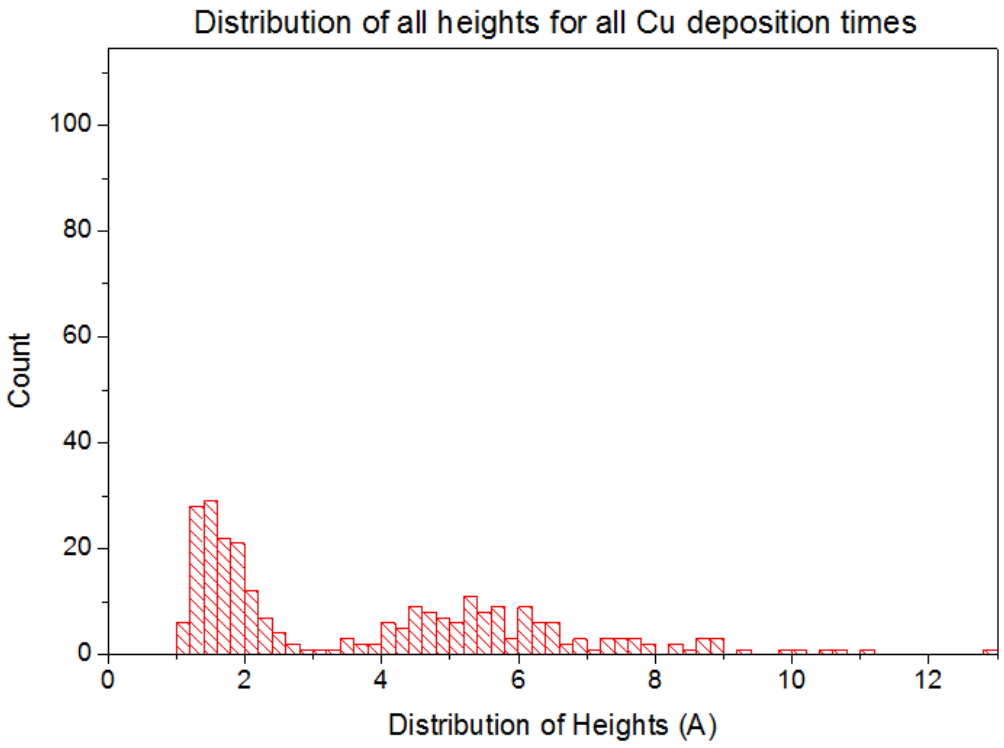

Figure 5-38 Distribution of all Cu cluster heights for all Cu depositions.

Using the lattice constant of 3.61 Å for Cu, the plane on which the Cu originated from be it (100), (110) or (111) could be determined by evaluating the distances between the peaks that occur and comparing them with the interatomic spacing calculated. Here is the interatomic spacing for each plane using lattice constant a = 3.61 Å;

- (100) = $\frac{a}{2}$ = 1.8 Å
- (110) = $\frac{a}{\sqrt{2}}$ = 2.55 Å
- (111) = $\frac{a}{\sqrt{3}}$ = 2.08 Å

From Figure 5-38 there appears to be peaks at 1.3 Å, approximately 4.5 Å and 5.4 Å. It is unclear from this data whether the peaks are separated by a factor of any of the both making it difficult to deduce which plane the Cu clusters originate from. This may be due to the limited height measurements for each deposition times. Approximately 50 heights where recorded for each deposition time. Increasing the height measurements to at least 100 might enable a better insight in to the preferred height and ultimately enable a determination of the Copper plane.

6 Summary and Conclusion

After detailed analysis of STM and LEED images of the clean surface the quasiperiodicity of the *i*-Ag-In-Yb sample has been confirmed. The crystal exhibits quasiperiodic rotational symmetry seen in both real LEED patterns and FFT analysis of the surface. The STM images proved the formation of the terraces from the annealing process. These terraces exist on the planes where the RTH clusters have been intersected perpendicular to the five-fold axes, enabling LEED and FFT patterns to be observed. The measurements of the step and terrace morphology have also shown that this particular *i*-Ag-In-Yb crystal compares well to samples from other experiments.

At low Cu coverage, the STM images shown Cu clusters began to form on the surface. The images obtained a low coverage were of good resolution and large uniform clusters could be clearly seen on the surface of the *i*-Ag-In-Yb. Varying between negative and positive bias voltage, the characteristic Ag & In protrusions and the Yb rings could be viewed and were measured in good agreement with previous *i*-Ag-In-Yb structural studies. Due to the relatively low coverage of Cu, the clean surface protrusion diameter and separation along with the ring diameter were still able to be studied. These measurements of the structural properties of *i*-Ag-In-Yb in comparison to previous measurements once again confirm the quasiperiodicity of the sample used in this study. The resolution for the negative bias voltage images at 1 minute 50 second deposition was extremely good and the protrusions could be seen clear enough throughout the images so that they could be easily measured. The positive bias voltage images exhibiting the Yb rings however were not of the same quality of resolution making the ring diameter measurement limited. Over 100 protrusions were measured for the negative bias images at low coverage giving an accurate average of both protrusion separation and diameter. Due to the poorer resolution in the positive bias images only 20 rings were able to be measured accurately; more STM images at positive bias voltage at this coverage would need to be obtained to achieve a more accurate measurement.

The height and size of the Cu clusters were measured using images from all the Cu deposition times at low coverage. Using a high resolution negative bias voltage image after 1 minute 50 second deposition, the average height of the Cu clusters was measured to be 1.29(±0.13) Å which is expected as the radius of Cu is comparable to this. This suggests that at low coverage the clusters appear to only be one layer high and prefer to form in a lateral direction below certain coverage. The Cu clusters are more circular in shape at lower coverage allowing for easy measurement of the lateral size.

The Cu clusters at low coverage were found to absorb on the surface protrusions, mainly on protrusions making up pentagons on the surface of negative bias voltage images. This compared well with the review of the quasicrystal model of the surface terminating bulk plane. The rings seen in the

positive bias voltage tend to form in large pentagons around a cluster, which is also reflected in the quasicrystal model. The similarities between the characteristic structural properties seen at both voltages used in comparison to the Penrose tiling again confirms the quasiperiodicity and long range order the surface of the *i*-Ag-In-Yb sample in use.

At high Cu coverage the cluster heights and lateral sizes were again measured. The images shown an increased build-up of Cu clusters to the point where the substrate could no longer be seen. FFT images however maintained the five-fold symmetry seen from the clean surface. Height measurements gave a range of heights present at all deposition times used for high coverage. This spread of heights rather than a preferred height indicates the growth of 3-D islands on the surface. This suggests a strong Cu-Cu absorbate interaction which leads to the growth of a layer before the completion of the previous layer. The cluster lateral size although difficult to measure at the higher coverage, shown an increase in size with an increase in coverage. However in comparison to the height increase, the height of the Cu clusters increases at a much faster rate than that of the lateral size giving stronger indication that the 3-D growth mode is preferred. The Cu clusters appear to form at all deposition times with the shape of the clusters becoming increasingly irregular at the highest coverage making the lateral size measurements inaccurate. It is to be noted that at high coverage, the height of the features on the surface is much greater and due to the nature of STM analysis the tip may not be able to reach the complete depth between very high features making some height measurements inaccurate. STM is a measure of charge density and not the definitive position and with the more Cu clusters present at higher coverage the more charge density the STM tip will read. This makes the STM measurements slightly inaccurate.

Histograms of all the heights and lateral sizes confirmed the increase in the range of heights and lateral size at higher coverage suggesting the clusters move away from a preferred height and size above certain coverage.

To summarise, the *i*-Ag-In-Yb sample used for this study was found to possess long range aperiodic order upon clean surface studies. The surface exhibited the expected step terrace morphology and shown good comparison to the Large and Small step characteristics of previously studied quasicrystal samples. The structural parameters of the properties shown at both positive and negative bias agreed completely with previously measured values. The quasicrystal model representing the positioning of rings and protrusions in comparison to a Penrose tiling was also reflected in the low coverage studies, further proving that the sample used for this study possessed forbidden symmetry. The deposition of Copper at various coverage, gave strong indication that at low enough coverage the Cu forms clusters in a single layer until after a certain point 3-D islands begin to form due to a strong Cu-Cu interaction. It is clear from FFT patterns taken at 4 minute coverage the

Cu possesses long range order similar to the quasicrystal surface. The single element thin film over layer appears to possess quasiperiodical properties despite have a reduced chemical complexity.

7 Outlook

To confirm the quasicrytalline nature of Copper on the surface of *i*-Ag-In-Yb, LEED images of the single element thin film over-layer would need to be obtained. If the symmetries observed were comparable to the LEED images from just the clean surface then the Cu would be able to be determined as possessing long range quasiperiodic order on the surface of *i*-Ag-In-Yb.

The next step for further investigations would be to determine the point upon which 3-D islands begin to form. This could be done by increasing the number of deposition steps and taking repeat measurements of height and size at 30 second intervals between 1 minute 30 seconds and 4 minutes.

Appendix

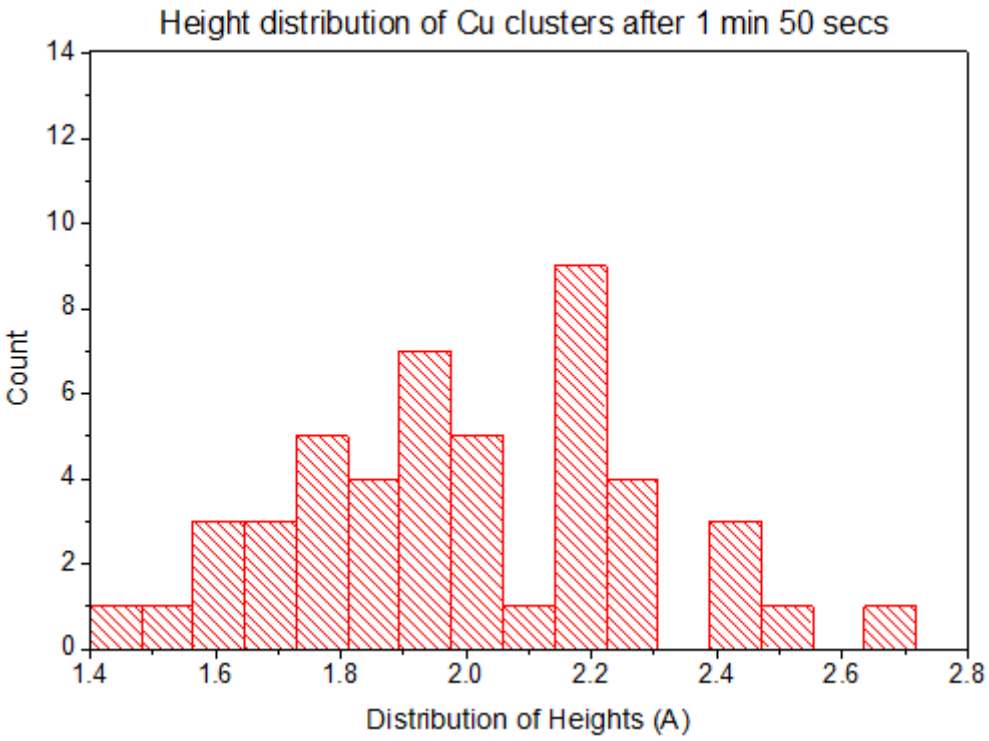

Figure 0-1 Height distribution of Cu clusters after 1 minute 50 seconds deposition.

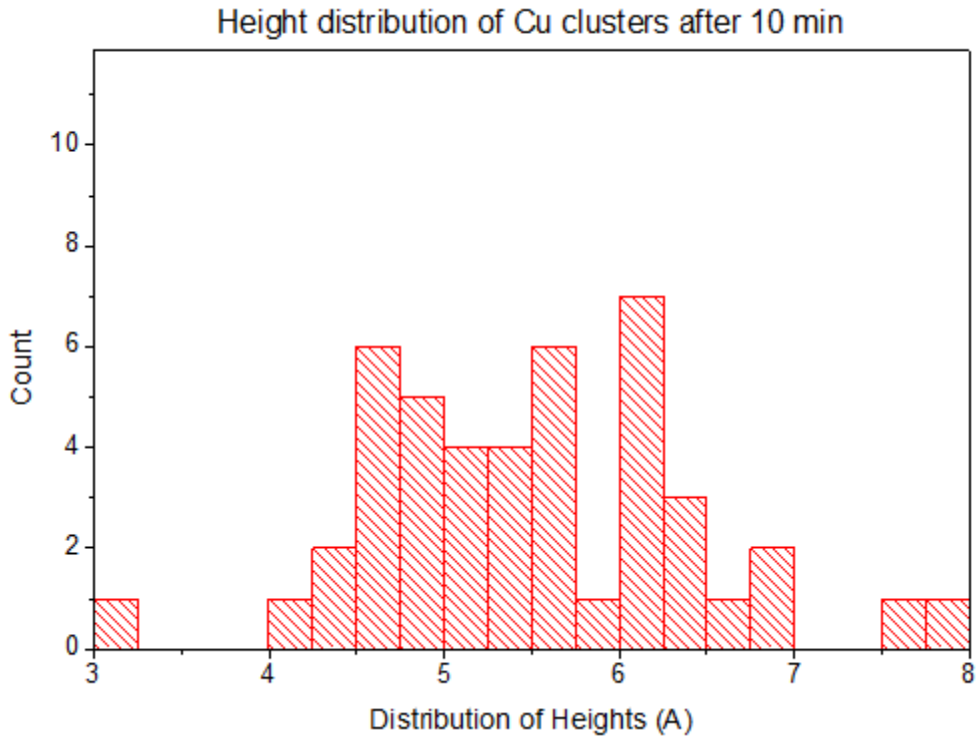

Figure 0-2 Height distribution o{{}}f Cu clusters after 10 deposition.

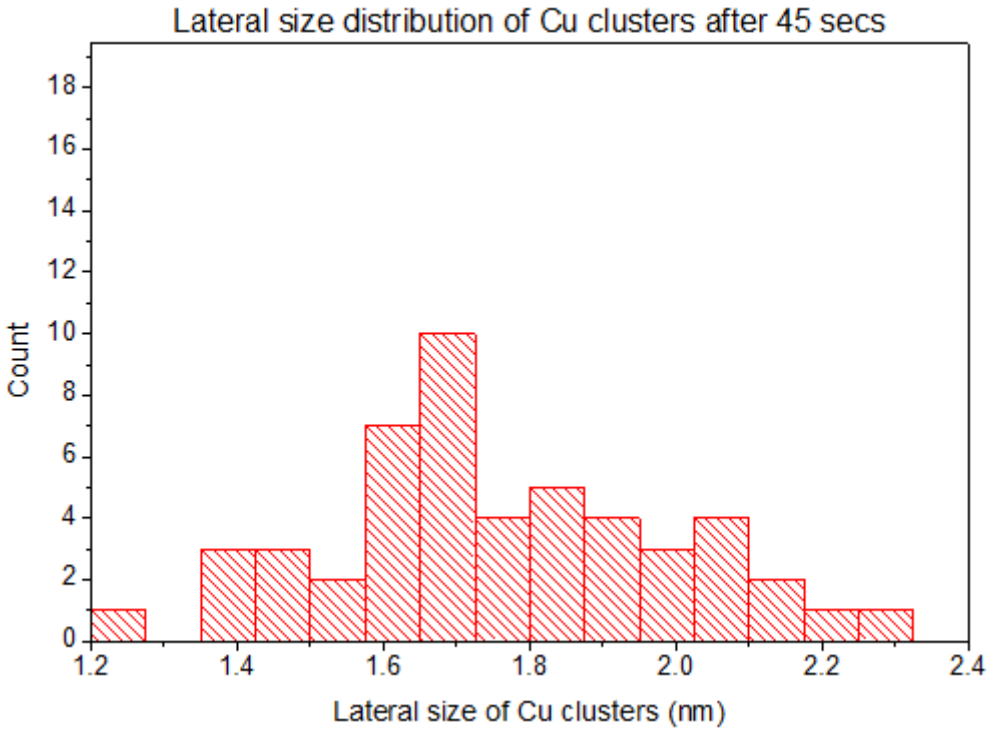

Figure 0-3 Lateral size distribution of Cu clusters after 45 seconds deposition.

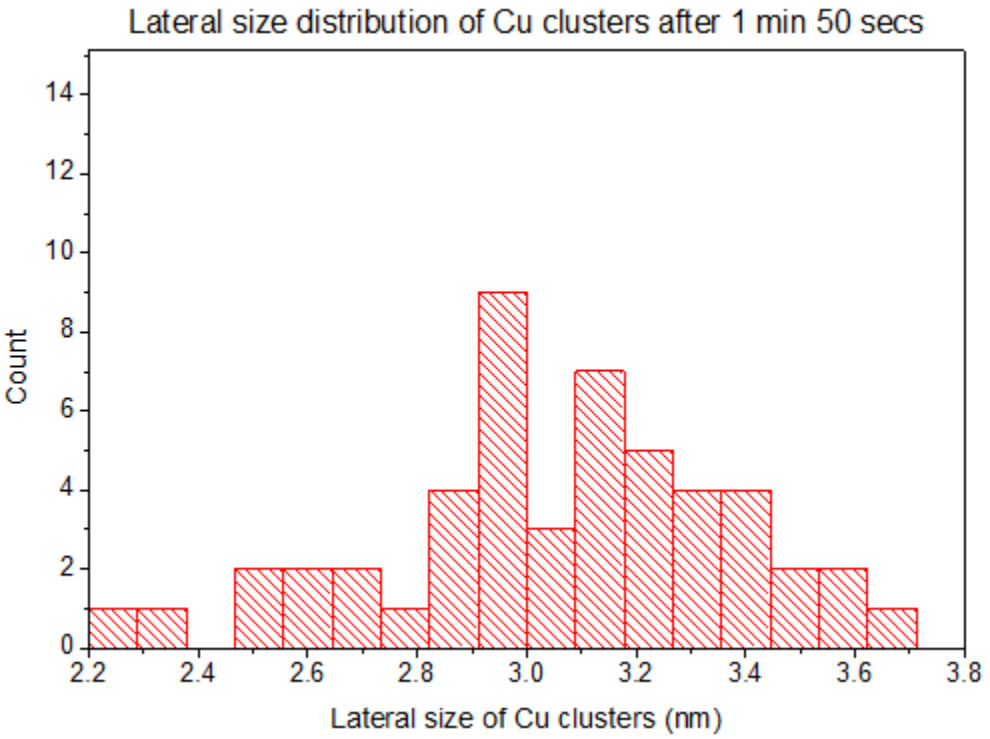

Figure 0-4 Lateral size distribution of Cu clusters after 1 minute 50 seconds deposition.

Acknowledgements

I would like to give my appreciation to Dr. H.R. Sharma for all his help and supervision during this study. A special thanks to Kirsty Young for her insight, guidance and most of all her time in helping me along with the UHV experiments and also the data analysis.

Bibliography

[1] SHARMA, H.R., SHIMODA, M., SAGISAKA, K., TAKAKURA, H., SMERDON, J.A., NUGENT, P.J., MCGRATH, R., FUJITA, D., OHHASHI, S. and TSAI, A.P., 2009. Structure of the fivefold surface of the Ag-In-Yb icosahedral quasicrystal. *Physical Review B - Condensed Matter and Materials Physics*, **80**(12),.

[2] SHARMA, H.R., SHIMODA, M. and TSAI, A.P., 2007. Quasicrystal surfaces: Structure and growth of atomic overlayers. *Advances in Physics*, **56**(3), pp. 403-464.

[3] NUGENT, P.J., SIMUTIS, G., DHANAK, V.R., MCGRATH, R., SHIMODA, M., CUI, C., TSAI, A.P. and SHARMA, H.R., 2010. Surface oxidation of the icosahedral Ag-In-Yb quasicrystal. *Physical Review B - Condensed Matter and Materials Physics*, **82**(1),.

[4] SHECHTMAN, D., BLECH, I., GRATIAS, D. and CAHN, J.W., 1984. Metallic phase with long-range orientational order and no translational symmetry. *Physical Review Letters*, **53**(20), pp. 1951-1953.

[5] SHARMA, H.R., 2002. "Structure, Morphology, and Dynamics of Quasicrystal Surfaces", Freie Universtat Berlin, Fachbereich Physik, 2002.

[6] KUO, Y.K., SIVAKUMAR, K.M., LAI, H.H., KU, C.N., LIN, S.T. and KAISER, A.B., 2005. Thermal and electrical transport properties of Ag-In-Yb quasicrystals: An experimental study. *Physical Review B - Condensed Matter and Materials Physics*, **72**(5),.

[7] SHARMA, H.R., SHIMODA, M., OHHASHI, S. and TSAI, A.P., 2007. First UHV surface studies of single-grain icosahedral Ag-In-Yb quasicrystal. *Philosophical Magazine*, **87**(18-21), pp. 2989-2994.

[8] ZIJLSTRA, E.S. and JANSSEN, T., 2001. Electronic properties of the three-dimensional Penrose tiling, *Ferroelectrics* 2001, pp. 381-384.

[9] SHARMA, H.R., NUGENT, P.J., SMERDON, J.A., SHIMODA, M., OHHASHI, S., FOURNÉE, V., LEDIEU, J. and TSAI, A.P., 2010. Impurity phases in icosahedral Ag-In-Yb quasicrystal: Influence in surface structure. *Journal of Physics: Conference Series*, **226**(1),.

I.Horcas et al. Rev. Sci. Instrum. 78, 013705 (2007)